NASA TECHNICAL MEMORANDUM

NASA TM X-74031

NASA TM X- 74031

(NASA-TM-X-74031)   DESIGN OF A LARGE   N77-23089
SPAN-DISTRIBUTED LOAD FLYING-WING CARGO
AIRPLANE (NASA)   99 p HC A05/MF A01 CSCL 01C
                                                    Unclas
                                          G3/05 26086

DESIGN OF A LARGE SPAN-DISTRIBUTED LOAD
FLYING-WING CARGO AIRPLANE

By

Lloyd S. Jernell
NASA Langley Research Center

and

C. Baptiste Quartero
Vought Corporation
Hampton Technical Center

April 22, 1977

This informal documentation medium is used to provide accelerated or
special release of technical information to selected users. The contents
may not meet NASA formal editing and publication standards, may be re-
vised, or may be incorporated in another publication.

NATIONAL AERONAUTICS AND SPACE ADMINISTRATION

LANGLEY RESEARCH CENTER, HAMPTON, VIRGINIA 23665

MAY 1977
RECEIVED
NASA STI FACILITY
INPUT BRANCH

1. Report No. NASA TM X-74031	2. Government Accession No.	3. Recipient's Catalog No.
4. Title and Subtitle DESIGN OF A LARGE SPAN-DISTRIBUTED LOAD FLYING-WING CARGO AIRPLANE		5. Report Date April 22, 1977
		6. Performing Organization Code 31.600
7. Author(s) Lloyd S. Jernell and C. Baptiste Quartero		8. Performing Organization Report No.
		10. Work Unit No.
9. Performing Organization Name and Address NASA Langley Research Center Hampton, VA 23665		
		11. Contract or Grant No.
12. Sponsoring Agency Name and Address National Aeronautics & Space Administration Washington, DC 20546		13. Type of Report and Period Covered Technical Memorandum
		14. Sponsoring Agency Code

15. Supplementary Notes

16. Abstract

The specifications for payload weight, density, and dimensions in essence configure the wing, forcing unusually low values of wing loading and aspect ratio. Wing-tip-mounted vertical tails provide a major increase in effective aspect ratio. Trim drag in cruise is negated by controlling the center of gravity by fuel management. A lift-drag ratio of nearly 19 is attained during cruise. For the design range, the fuel efficiency is approximately 50 percent greater than that of the most efficient current freighters.

The structural weight is only .18 percent of maximum gross weight because of the distributed loading.

Sufficient control power to counteract the large rolling moment of inertia dictates a relatively high minimum approach velocity of 315 km/hr (170 kts).

Despite the large values of gross weight and total thrust, the aircraft noise levels are reasonable. The major noise source is that of the airframe.

17. Key Words (Suggested by Author(s)) Advanced Cargo Aircraft, Span-Distributed Payload, Cargo Aircraft Design	18. Distribution Statement Unclassified-Unlimited		
19. Security Classif. (of this report) UNCLASSIFIED	20. Security Classif. (of this page) UNCLASSIFIED	21. No. of Pages 97	22. Price* $5.00

DESIGN OF A LARGE SPAN-DISTRIBUTED LOAD
FLYING-WING CARGO AIRPLANE

By Lloyd S. Jernell.
NASA Langley Research Center

and

C. Baptiste Quartero
Vought Corporation
Hampton Technical Center

SUMMARY

The specifications for payload weight, density, and dimensions in essence configure the wing, forcing unusually low values of wing loading and aspect ratio. Wing-tip-mounted vertical tails provide a major increase in effective aspect ratio. Trim drag in cruise is negated by controlling the center of gravity by fuel management. A lift-drag ratio of nearly 19 is attained during cruise. For the design range, the fuel efficiency is approximately 50 percent greater than that of the most efficient current freighters.

The structural weight is only 18 percent of maximum gross weight because of the distributed loading.

Sufficient control power to counteract the large rolling moment of inertia dictates a relatively high minimum approach velocity of 315 km/hr (170 kts).

Despite the large values of gross weight and total thrust, the aircraft noise levels are reasonable. The major noise source is that of the airframe.

INTRODUCTION

Studies by both NASA and the aircraft industry are currently being conducted to determine the problems associated with the design and operation of very large, long-range, subsonic cargo aircraft. Such aircraft use large cargo containers and have a payload capability much greater than that of present aircraft. A design concept which holds promise for such an airplane is that of distributing the payload along the wingspan to counterbalance the aerodynamic loads, with a resultant decrease in the in-flight wing bending moments and shear forces. It is expected that this decreased loading of the wing structure, coupled with the very thick wing housing the cargo would result in a relatively low overall structural weight in comparison to that of conventional aircraft.

However, there are many potential problem areas associated with this type of aircraft, including aerodynamic efficiency, control (particularly in roll due to the high moment of inertia about that axis), and airport handling because of its large size. In order to evaluate some of these unknowns, the preliminary design of a large distributed-loading cargo airplane was performed. This work was conducted by the Vought Corporation - Hampton Technical Center, under the technical direction of the Vehicle Integration Branch, Aeronautical Systems Division, Langley Research Center. The results of this study are summarized herein.

Other studies pertaining to the span-distributed loading cargo aircraft concept are documented in references 1 to 4.

SYMBOLS AND NOTATION

A	aspect ratio
b	wingspan
c	local chord
$\bar{c}$	mean aerodynamic chord
c.g.	center of gravity
c_a	speed of sound at ambient conditions
c_r	rudder local chord
c_{vt}	vertical tail local chord
C_D	drag coefficient, $\frac{Drag}{qS}$
C_L	lift coefficient, $\frac{Lift}{qS}$
$C_{m.25\bar{c}}$	pitching-moment coefficient about $0.25\bar{c}$
C_n	yawing-moment coefficient, $\frac{Yawing\ moment}{qSb}$
C_{n_β}	directional stability parameter, $\frac{dC_n}{d\beta}$, per deg
D	diameter, also drag
EPNL	effective perceived noise level
F_b	blade passing frequency
g	gravitational constant

2

h	altitude, also height of vertical tail
HSAS	hardened stability augmentation system
L	lift
L/D	lift-drag ratio
M	Mach number
MLW	maximum landing weight
M_x'	swept-wing-axes net limit bending moment
$M_{y_{ea}}'$	net limit torsion about wing-box elastic axis
NB	number of fan blades
OASPL	overall airframe sound pressure level
OWE	operating weight, empty
q	dynamic pressure
q_s	wing-box-skin shear flow
q_v	wing vertical beam shear flow
q_{web}	beam-web shear flow
R	radius
rpm	revolutions per minute
RLW	reserve-fuel landing weight
S	wing area
SPL	sound pressure level
S_z'	swept-wing-axes net limit shear
$T_{T,a}$	ambient total temperature
$T_{T,jet}$	jet total temperature
TSFC	thrust specific fuel consumption
t	thickness, also time

t_2	time to double amplitude
t/c	wing-section thickness ratio
V	velocity, also vertical shear
V_{cw}	cross-wind velocity
W	gross weight
X	axis parallel to nacelle centerline
Y	cross-section neutral axis
ZFW	zero fuel weight
α	angle of attack, referenced to airfoil centerline, deg
β	angle of sideslip, deg
δ_e	elevon deflection, positive for trailing edge down, deg
δ_f	flap deflection, deg
δ_r	rudder deflection, positive for trailing edge left, deg
$\S$	damping ratio
η	wing station, measured from fuselage centerline along centerline of wing box
ϕ	roll angle, deg
ω_n	natural frequency

Subscripts:

elastic	non-rigid structure
max	maximum
min	minimum
rigid	rigid structure
trim	trimmed condition

BASIC DESIGN CRITERIA

The study required the preliminary design of a span-distributed loading airplane capable of transporting large containers of cargo over transcontinental distances. Due to the limitations of available data, manpower, and time, the study was restricted in scope as much as practicable; hence, many of the fundamental configuration, mission, and performance specifications set forth were chosen intuitively. The basic design criteria were as follows:

Configuration - flying wing, with wingtip vertical tails and a relatively small fuselage for flight deck and crew accommodation.

Wing planform - 30-degree sweep, no taper.

Airfoil - t/c = 0.20, one of several Langley-developed airfoils or modifications thereof.

Cargo-compartment dimensions - sufficient to handle 2.44 m x 2.44 m (8 ft x 8 ft) cargo containers of assorted lengths.

Payload weight - 272,155 kg (600,000 lbm).

Payload density - 160.2 kg/m^3 (10 lbm/ft^3), including container.

Propulsion - current-production turbofan engines, scaled if necessary.

Range - 5,926 km (3,200 n.mi.).

Cruise Mach number - at least 0.7.

Runway length - 3,658 m (12,000 ft) maximum.

Cargo-compartment pressurization - none.

Cargo loading location - wingtips.

CONFIGURATION DEVELOPMENT

The final configuration is shown in figure 1. The following sections give a description of the configuration and the fundamental design philosophy.

Wing

Planform.- Having specified sweep, taper ratio, container size, and payload weight and density, the remaining criteria pronouncedly affecting overall wing geometry were airfoil shape and cargo arrangement. Since the airfoils under consideration were similar in thickness distribution, cargo arrangement was

5

the first variable studied to establish the approximate wing planform. Configurations accommodating two, three, and four rows of containers parallel to the wing leading edge were considered. The two-row configuration provided an aspect ratio of approximately 7.6, but required a span of roughly 440 feet It was felt that a span of this magnitude not only would pose serious runway and cargo-terminal compatability problems, but would also exact considerable structural-weight penalty in order to assure sufficient wing stiffness for maximum maneuver and taxi loads.

In contrast, the four-row arrangement reduced the required span to approximately 215 feet, but also reduced the aspect ratio to approximately 3.1. This configuration obviously would have lower aerodynamic efficiency due to the higher induced drag coefficient. Consequently, the three-row configuration, having a refined span of 290 feet and a geometric aspect ratio of approximately 4.4, was chosen as having the best compromise between structures, aerodynamics, and ground operations.

It should be pointed out that the specifications for payload weight, density, and dimensions in essence configure the wing and establish the wing loading. No attempt was made to employ twist as a means of altering the spanwise load distribution since this would require either larger payload-structure clearances or create loading problems due to an unlevel cargo floor. It was determined early in the study that the configuration would have a wing loading of only about 342 kg/m^2 (70 lbm/ft^2). Although it follows that, because of the low span loading in comparison to conventional aircraft, the configuration would have relatively low induced drag, it also would exhibit relatively high profile drag due to the large wetted area and high thickness ratio.

Airfoil.- The airfoil selection was based primarily on the need for a two-dimensional critical Mach number of approximately 0.7, very low pitching moment, and maximum utilization of wing volume for the cargo compartment. Data on supercritical airfoils developed to date indicate that this type of profile would meet the cruise speed and volume-utilization requirements; however, most supercritical airfoils inherently display large negative pitching moments because of the relatively severe rearward camber.

Limited research has been conducted at the Langley Research Center on thick airfoils applicable to spanloaded aircraft. These airfoils typically have the large leading-edge radius and thickness distribution characteristic of supercritical airfoils, but are cambered so as to provide low pitching moment. Two airfoils were selected as candidates for application to the present design study. One utilized a moderate amount of positive camber over approximately the forward 70 percent of the chord, but was reflexed over the remaining rearward section to provide an essentially zero pitching moment about the quarter-chord. The other airfoil was a modification of an early supercritical airfoil in which the camber was removed and the thickness ratio increased to 0.20.

Early in the design study, unpublished wing-tunnel data became available on a 30-degree sweep, distributed-load cargo aircraft model incorporating the reflexed airfoil. These data indicated that at cruise Mach number and angle of attack, boundary-layer separation existed over roughly the rearward 30 percent of the

6

upper surface (the region of the reflexed surface). Sufficient data were not available to ascertain whether the separation was a Mach number effect or due simply to the low test Reynolds number. Furthermore, theoretical data from the analysis program of reference 5 (which computes the flow field about an airfoil at supercritical Mach numbers) predicts that, for an assumed lift coefficient of 0.40, the drag-rise Mach number for the reflexed airfoil is 0.03 less than that for the symmetrical airfoil. In addition, preliminary layouts of the wing structure for both airfoils showed that the symmetrical airfoil was slightly more efficient in terms of wing volume utilization for the cargo compartment. Hence, the symmetrical airfoil was selected for the design study.

Dihedral.- A wing dihedral angle of 3 degrees was employed to alleviate the need for the relatively long main landing gear required to provide for ground clearance of the wingtip and deflected elevon during landing and takeoff.

Fuselage

The fuselage was originally configured solely for flight deck, crew accommodation, and nose gear. However, it was later found necessary to install a fuel tank in the unused volume so as to provide a greater range of center-of-gravity management.

Vertical Tails

The wing-tip-mounted vertical tails, designed according to the suggested guidelines of reference 6, have a quater-chord sweep of 30 degrees, a taper ratio of 0.30, and an aspect ratio of 2.31. The airfoil used is an eight-percent-thick modification of the GA(W)-1 airfoil (17-percent thickness) described in reference 7. The nonplanar lifting surface method of reference 8 was used to optimize cant and toe-in angles of the fins for the best combination of aerodynamic efficiency and structural weight.

Engines and Nacelles

The configuration has six turbofan engines (scaled from the JT9D-7 engine) to provide the required thrust. The engines, mounted on pylons above the wing, were originally positioned such that roughly 80-percent of the nacelle was ahead of the wing leading edge. Later it was necessary to move the nacelles rearward to lessen the large adverse effect of the nacelles and pylons on directional stability as well as to avoid possible adverse interference drag from struts located within the supercritical flow region of the upper surface of the wing. In the final position, the nacelle inlet lip is located at approximately the 35 percent local-chord station.

Controls and High-Lift System

The elevons have a chord equal to 20 percent of the wing chord, and extend from the 60 percent semispan station to the vertical tails. Maximum elevon deflection is +40 degrees. The spoilers, required to augment roll control because of the high inertia in roll, have a chord equal to 15 percent of the wing chord and are located as shown in figure 1. The non-split rudders have a chord equal to 20 percent of the vertical-tail local-chord and a maximum deflection of +40 degrees. The high-lift system consists of simple trailing-edge flaps having a chord equal to 15 percent of the wing chord and extending from the wing centerline to the 60 percent semispan station. Maximum flap deflection is 20 degrees.

Fuel System

The fuel tanks are located as shown in figure 2. The wing tanks are positioned ahead of the front wing box beam and behind the rear beam. The forward tanks extend outward to the 50 percent semispan station, whereas the rearward tanks extend to the inboard main gear wheel wells. The fuselage tank was provided to widen the range of control over the center-of-gravity.

Landing Gear

The landing gear is composed of a twenty-wheel, four-strut main gear and a two-wheel nose gear. The inboard pair of main gear, utilizing six-wheel bogies, are located rearward of the wing-box rear beam at approximately the 33 percent semispan station. The outboard gear have four-wheel bogies and are positioned forward of the wing box front beam at approximately the 77 percent semispan station. To facilitate landing load distribution, the oleo-pneumatic suspensions of the pair on each side are interconnected. A landing gear of this configuration might require steering of at least one pair of main gear; however, such an analysis was beyond the scope of this study.

STRUCTURES

Since all structural components other than the wing box are of conventional design, the structural analyses of these items were confined to component layout and determination of mass properties using statistical data. Because of the unique geometry and loading requirements of the wing, a detailed study was performed wherein the wing-box structural concept was developed and the dimensions of its structural components were analytically determined.

The final wing-box design, shown in figure 3, incorporates conventional stiffened, stressed-sheet structure constructed primarily of 2024-T3 aluminum, with 7075-T6 aluminum being employed where the higher allowable stress can be used to advantage. Two vertical beams, reinforced by vertical stiffeners, are connected by beam-type upper and lower rib-caps which, in turn, are

supported by tension tubes located between the cargo bays. The rib-caps support the stringer-stiffened wing skins. The lower rib-caps also support the spanwise beams of the cargo subfloor. Figure 4, which shows a cross-section of the wing normal to the leading edge, provides additional details of the wing box at a typical rib station.

Maximum design loads criteria established early in the study are:

- 2.5 g balanced flight maneuver at maximum gross weight and cruise Mach number and altitude.

- 2.0 g taxi at maximum gross weight.

In additional, the final structural analysis is based on the following conditions:

- Maximum design gross weight of 617,158 kg (1,360,600 lbm).

- For 2.5 g flight maneuver, c.g. located at 0.29 $\bar{c}$, M = 0.75, altitude = 8,595 m (28,200 ft).

- For 2.0 g taxi, c.g. positioned at 0.34 $\bar{c}$.

The procedures employed in the design of the wing box are based on the methods of reference 9. Although the analyses are of comparatively limited scope, the results are considered adequate for preliminary design purposes. The values of wing shear, bending moment, and torsion, calculated for the maximum-design-load conditions, are shown in figures 5, 6, and 7, respectively. The airloads for 2.5 g flight maneuver were calculated using the computer program of reference 8.

Due to the relatively simple wing-box geometry and the desire to minimize component gage changes, structural analyses were conducted only at the six semispan stations shown in figure 8. As will be noted, two stations represent the ribs supporting the inboard and outboard main gear; the remaining four stations were chosen intuitively. A shear flow diagram similar to that of figure 9 was generated at each station to determine beam-web and skin thicknesses.

The vertical shear is distributed equally between the two vertical beams. The beam webs are permitted to buckle, and are designed to carry the vertical shear and the wing-skin shear flow due to torsion with the webs in the diagonal tension-field condition. The variation of web thickness along the structural semispan is shown in figure 10. The web stiffeners, spaced at 38.10 cm (15 in) intervals, are of the geometry shown in figure 11. The spanwise variation of stiffener cross-sectional area is presented in figure 12.

The beam caps, stringers, and skins are designed to carry all bending loads. In addition, the skins, which are allowed to buckle, also support the chordwise shear loads due to torsion. Hence, the sizing of these components and determination of stringer spacing required several iterations. The loads on the

beam caps and stringers (including effective skin) were calculated at the six semispan stations using a distance of 307.34 cm (121.00 in) between beam-cap centroids and an average distance of 365.76 cm (144.00 in) between stringer centroids. Sectional geometries of these components are shown in figure 11. The spanwise variation of beam-cap and stringer cross-sectional areas are presented in figures 13 and 14, respectively. For a given skin thickness, the allowable buckling chordwise shear stress is proportional to stringer spacing; therefore, the close stringer spacing (20.42 cm (8.04 in)) allows a relatively high buckling stress. The variation of skin thickness along the semispan is shown in figure 15.

The wing-box structure includes one hundred thirty (130) frame-type ribs. In addition, four beam-type ribs of heavier forged aluminum are located at the main-gear attachment points. All ribs are spaced at 76.20 cm (30.00 in) intervals. The upper and lower I-beam rib caps are designed for the load resulting from the 2.5 g flight maneuver. The analysis and sizing were performed only at wing station 2001.32 cm (787.92 in), which is the location of the rib supporting the inboard main gear. The rib-cap loads at this point were assumed to be typical of those throughout the wing box.

The cargo subfloor structure consists of the lower rib cap, which also serves as the main chordwise subfloor beam, and four spanwise beams located below each of the three cargo bays. The spanwise beams, consisting of upper and lower caps and stiffened webs, have a 25.40 cm (10.00 in) depth determined by design layout. No structural analyses were performed on the subfloor components.

Although the study airplane exhibits a low ratio of structural weight to gross weight in comparison to conventional cargo aircraft, weight reduction is limited since neither weight nor the external loads are uniformly distributed along the span. Component weights of such items as propulsion units, fuel and tanks, and landing gear cause considerable spanwise variation of weight, and realistically, even the assumed uniform distribution of payload weight is an ideal case which would rarely be encountered. With regard to external loads, the airloads are not uniform due to the aforementioned impracticability of utilizing wing twist. Also, landing and taxi loads are highly concentrated and tend to limit maximum loads to some extent. The results of the studies indicated that the extreme depth of the spars is not as advantageous as might be expected since the failure modes occur in buckling with very low maximum allowable stress. Preliminary estimates, wherein extrapolations of empirical data were utilized, indicated a wing structural weight of approximately 29 kg/m^2 (6 lbm/ft^2); however, detail design studies predicted an all-aluminum weight of approximately 43.0 kg/m^2 (8.8 lbm/ft^2). Further studies wherein it was assumed that 90 percent of the wing secondary structure, control surfaces, and flaps could be constructed of epoxy composite material indicated that the overall wing weight could be reduced to 41.0 kg/m^2 (8.4 lbm/ft^2).

MASS PROPERTIES

The mass properties analysis consisted of the determination of aircraft weights, moments of inertia and center-of-gravity ranges. Mass properties of the wing box were obtained analytically using data generated during the structural design. Those of the wing secondary structure, control surfaces, and flaps were estimated using statistical data, with an adjustment for a 20-percent component weight reduction through the use of epoxy composite material for 90 percent of the structure. The fuselage properties are those of a typical subsonic transport forebody, adjusted for structural modification due to the increased loads of the nose gear and fuselage fuel tank. Data for the vertical tails, landing gear, nacelles, and fuel system were obtained statistically with the use of the Vought-Hampton ESBULL computer program. The mass characteristics of the scaled JT9D-7 engines were calculated with the use of engine data and scale factors provided by the manufacturer. Mass properties of all other items were obtained from data for a large commercial transport currently in operation, with adjustments applied where appropriate.

The weight breakdown by component and by group is listed in Table I. The airplane has an operating empty weight of 175,359 kg (386,600 lbm) and a design gross weight of 617,158 kg (1,360,600 lbm). A bar graph of the weight breakdown is provided in figure 16. The structural weight comprises only about 18 percent of the maximum gross weight, exemplifying the magnitude of structural efficiency achievable through the utilization of the span-distributed loading concept.

The moments of inertia about the stability axes and the product of inertia about the principal axis are presented in Table II for several significant conditions. Of course, the roll and yaw inertial moments are much greater than those of conventional cargo aircraft which carry the payload in the fuselage.

The center-of-gravity gross-weight envelope is presented in figure 17 for an assumed uniform design-payload distribution, and also for the ferry mission. The forward c.g. limit represents the restriction imposed by the available control power for aircraft rotation during takeoff. The rearward limits represent dynamic lateral-directional restrictions. As will be noted, for both the design-payload and ferry missions, the rearward dynamic limits during the approach mode severely restrict utilization of the reserve fuel. However, the resolution of this problem was not pursued due to the limited scope of the study. The optimum cruise c.g. position (zero elevon deflection) is $0.29\bar{c}$. The fuel distribution for various points on the c.g.-GW envelope are presented in Table III.

AERODYNAMICS

Due to the high span and inherent low wing loading associated with this configuration, both span and chord were held to the minimum required for cargo containers,

container clearance, and structural thickness. Based on the results of the final structural analysis, values chosen for the span and streamwise chord are 88.39 m (210.00 ft) and 19.51 m (64.00 ft), respectively. The resultant aspect ratio is 4.53.

In comparison to current cargo aircraft, the configuration has numerous unconventional features which affect the aerodynamic characteristics, including the low values of wing loading and aspect ratio, a high section thickness ratio, wing-tip-mounted vertical tails, and no horizontal tail.

In comparison to conventional cargo aircraft, the study airplane exhibits relatively low induced drag due to the low span loading. However, the configuration develops relatively high profile drag due to the large wetted area and high thickness ratio. Also, the high thickness-ratio wing posed a design challenge due to the large adverse pressure gradients over the rearward surfaces at cruise conditions, which resulted in an increased tendency for flow separation. The resolution of the separation problem was complicated by the requirement for very low pitching moment, which negated full implementation of supercritical airfoil technology. In the latter part of the study an effort was made to employ a small amount of camber to improve the aerodynamic efficiency; however, this approach was abandoned because the rearward static c.g. limit was determined to be ahead of the forward limit. Friction drag was calculated by standard methods, using flat plate turbulent friction coefficients adjusted for the effects of supervelocity, interference, protuberances, gaps, and boundary-layer separation near lifting-surface trailing edges. Nacelle drag was also adjusted for boat-tail effects and loss of leading-edge suction.

The induced drag was calculated using the method of reference 8. In this method the configuration was represented as planar surfaces conforming to the camber planes of the wing and vertical tails. Although the geometric aspect ratio is only 4.53, the effect of the wing-tip-mounted vertical tails is to increase the effective aspect ratio to approximately 7.9.

A tailless design incurs large trim drag penalties if the trimming moments are obtained by means of the elevons. This effect is even more pronounced in the present configuration since a moderate upward deflection of the elevon significantly decreases the induced efficiency increment of the vertical fin. Thus trim is obtained by fuel management where fuel is pumped between tanks so as to force the elevon deflection to zero. In cruise, trim drag is zero. At takeoff and landing, dynamic stability limits the allowable travel of the center of gravity. Appropriate trim-drag penalties were assessed against the aircraft in the landing and takeoff configurations.

The increase in drag due to localized supersonic flow was determined from two-dimensional airfoil calculations using the computer program of reference 5. Adjustments were made for three-dimensional effects using simple sweep theory. Drag-rise increments of the fuselage, and engine nacelles and pylons were neglected since sufficient experimental data were not available.

The lift characteristics, including flap and elevon deflections, were obtained using the computer program of reference 10. This method calculates the aerodynamic characteristics of wing-body tail combinations in subsonic and supersonic potential flow. The wing and fuselage of the configuration are represented as a large number of panels each of which contains aerodynamic singularities. The engine nacelles and pylons were not included in the input geometry. The method of reference 11 was employed to account for the effects of engine exhaust on cruise lift and drag.

Lift-drag polars, with and without ground effect ($h/b \approx 0.1$ and $h/b \geq 1$), are shown in figures 18 and 19 for the landing and takeoff modes, respectively. A flap deflection of 20 degrees is used for both takeoff and landing. The difference in polars for the two flight modes is due to thrust effects on trim requirements. Figure 20 presents the variation of lift with angle of attack for the aforementioned flight conditions.

Cruise lift-drag polars are shown in figure 21. The corresponding lift-drag ratios are shown in figure 22. The curve for $M = 0.75$, which has maximum lift-drag ratio of 19.00, compares favorably with the combination of lift-drag ratio ($L/D = 18.65$) and specific fuel consumption actually achieved in cruising flight. As will be discussed subsequently, these optimum values correspond to the maximum range as determined from the Breguet range equation.

STABILITY AND CONTROL

The static and dynamic analyses of the aircraft stability and control are based on the data of reference 12, the previously discussed aerodynamic and mass-properties data, and the methods of reference 13.

Criteria

The criteria employed in determining the stability and control requirements were obtained from reference 14, with the exception of the longitudinal dynamic guidelines, which are based on unpublished data. The longitudinal criteria are as follows:

- For all weights and c.g. positions, the time to double amplitude shall be greater than two seconds.

- The forward c.g. position during takeoff shall be determined by the ability to maintain takeoff lift coefficient and to provide the required control power for aircraft rotation.

13

- The rearward c.g. position during approach shall be determined by the ability to provide a nose-down pitching acceleration of 0.08 rad/sec^2 at minimum demonstrated velocity and maximum gross weight.

The criteria for determining the lateral-directional stability and control requirements are as follows:

- The aircraft shall have positive effective dihedral.

- The aircraft shall be directionally stable for all flight modes.

- There shall be adequate on-the-ground directional control to provide trim in a 56 km/hr (30 kt), 90-degree cross wind.

- The minimum cross-wind control velocity shall be sufficiently low to allow nose-wheel steering.

- There shall be adequate directional control to counteract an outboard engine failure at maximum-thrust engine-failure velocity.

- At approach velocity, the lateral control shall be sufficient to provide a roll-response capability of 30 degrees within 2.5 seconds after initiation of a rapid, full-lateral-control input.

- At approach velocity, the directional control shall be capable of providing a side-slip angle of 10 degrees with not more than 75 percent of full lateral control required to maintain wings-level flight.

- The aircraft shall have an inherent Dutch-roll stability, with an undamped natural frequency of at least 0.4 rad/sec.

Longitudinal Stability and Control

The estimated control capabilities of the aircraft for an elevon-deflection range of $\pm$40 degrees and a c.g. position of 0.25$\bar{c}$ are shown in figures 23 to 25 for the cruise, initial climb-out, and approach modes, respectively. Flap deflections employed were zero for cruise, and 20 degrees for both climb-out and approach. The data exhibit the pronounced effect of elevon deflection on lift coefficient. In fact, upon comparing elevon and flap size, it is obvious that the variations of lift and drag due to elevon deflection are of the same order of magnitude as those resulting from flap deflection. Hence, where practicable, aircraft trim should be accomplished by c.g. management rather than elevon employment. However, for the initial climb-out and for approach modes, which require high lift

coefficients, the c.g. should be positioned at the rearward limit in order to maximize available lift for maneuvering.

Estimates of elevon deflection required to trim the aircraft for various c.g. positions during initial climb-out, cruise, and approach are presented in figure 26. It will be noted that cruise-mode trim with zero elevon deflection requires a c.g. position of approximately $0.29\bar{c}$. The data also show the significant effect of c.g. position on elevon deflection required for trim during climb-out and approach.

The longitudinal-control capabilities for the climb-out and approach modes are replotted in figures 27 and 28, respectively, along with the statically determined limits for c.g. travel and the corresponding trimmed lift coefficients. The climb-out forward static c.g. limit of $0.28\bar{c}$ was determined by the control power required to rotate the aircraft at a velocity of 263 km/hr (142 kt). The rearward static c.g. limit for both climb-out and approach is $0.50\bar{c}$ and is based on the ability to provide a nose-down pitching acceleration of 0.08 rad/sec^2 at minimum demonstrated velocity and maximum gross weight. The approach forward static c.g. limit of $0.23\bar{c}$ is not determined by maximum control power, but on the ability to attain a lift coefficient 1.5 times the approach lift coefficient. Since the aircraft is statically unstable over most of the c.g. range, a Hardened Stability Augmentation System (HSAS) is required for stability.

Controls-fixed dynamic analyses of the aircraft were conducted for the climb-out and approach modes. The estimated time required to double amplitude as a function of c.g. position is shown in figure 29. According to unpublished data, a two-second minimum time to double amplitude is the limit for which a current HSAS would be able to provide adequate stability. The resulting rearward c.g. limit for the initial climb-out at maximum gross weight is $0.309\bar{c}$. For the approach mode, the rearward limits are $0.304\bar{c}$ and $0.318\bar{c}$, respectively, for the maximum and reserve-fuel gross weights. These limits, which impose greater restrictions on rearward c.g. travel than the aforementioned static limit, prevent the use of optimum elevon settings during takeoff and landing. Therefore, efficient operation of the aircraft in these flight modes would require the development of a very rapid-reaction (or fast-response) control system. However, such a system, which might include small secondary surfaces on the elevons, was not analyzed in the present study.

The rearward dynamic c.g. limit for the clean configuration during the climb and acceleration mode is shown in figure 30 (for the minimum time of two seconds to double amplitude). The rate of change of the rearward limit with aircraft velocity is sufficiently low to allow the use of fuel transfer for maintaining the c.g. within the required limits.

Lateral-Directional Stability and Control

The methods of reference 13 were employed in determining the lateral-directional characteristics. Although the engine nacelles and pylons generate a large part

15

of the side force, these components have a relatively small effect on yawing moment since their longitudinal position is near the aircraft c.g. The vertical tails are considerably larger than required to meet the criterion that $C_n > 0$; however, tail design was not based on directional stability minimum requirements. Instead, the tails were designed primarily to increase induced efficiency by following the winglet-design guidelines (ref. 6).

Figure 31 exhibits the effects of control deflection and local rudder-tail chord ratio on the directional control capability of the aircraft. Also shown is the minimum control power necessary to meet the requirement of maintaining a straight flight path during takeoff with an outboard engine inoperative. Based on these data, a rudder-tail chord ratio of 0.2 and a maximum deflection of ±40 degrees were selected.

The lateral response of the aircraft was estimated by solving the single-degree of- freedom equation of motion in roll for a step-control input. The results are presented in figure 32 for the three levels of flying-qualities requirements specified in reference 14. The data indicate that the airplane has satisfactory roll response at an approach velocity greater than 315 km/hr (170 kt); this is a considerably higher velocity than desirable. The level-2 requirement can be met at a velocity of 248 km/hr (134 kt). These speeds, rather than maximum lift, control the aircraft approach speed. A lower approach velocity could be attained by a roll-response requirement reduced from those of reference 14. Extensive development of more powerful lateral control systems would be necessary to further reduce the landing speed; however, such development is beyond the scope of a preliminary design study.

The ability of the aircraft to meet steady-sideslip trim requirements during takeoff and landing was estimated by solving the two-degree-of-freedom equations for roll and yaw steady-state trim. The results indicate that 36 percent of the maximum rudder deflection and 46 percent of the maximum elevon deflection are required to maintained a wings-level approach with a 10-degree sideslip angle. This is well within the specified allowable limit of 75 percent maximum control deflection.

Figure 33 shows the minimum elevon and rudder deflections required for lateral and directional control during the takeoff ground run with a 56 km/hr (30 kt), 90-degree cross wind. It will be noted that adequate control is available about both axes at a minimum velocity of 145 km/hr (78 kt). Control at lower velocities can be accomplished by nose-wheel steering.

An examination of the roots of the characteristic equation of motion indicates that the airplane has acceptable spiral and Dutch-roll modes and a marginally acceptable roll-damping mode. The roll-mode time constant is acceptable for maximum gross weight, but is slightly too large for the reserve-fuel gross weight. Table IV presents a comparison of the inherent lateral-directional characteristics of the airplane with the assumed requirements.

PROPULSION

The engines selected for the study are scaled JT9D-7 turbofans which have been sized to provide an installed static thrust of 240,200 N (54,000 lbf) each at sea-level, standard-atmosphere conditions. The engine is of two-spool, axial-flow design with high bypass and compression ratios. The production-engine ambient-temperature ranges for constant-thrust power settings, as recommended by the manufacturer, are as follows:

Takeoff power - standard day +12 C and below.

Maximum climb power - standard day +10 C and below.

Maximum cruise power - standard day +15 C and below.

Constant-thrust operation above standard-day temperature results in a considerable increase in fuel consumption. A detailed description of the production engine, along with basic performance data, is presented in reference 15.

The unscaled, installed engine performance data were generated by correcting the basic performance data for inlet recovery, service airbleed, and auxiliary-power extraction using the methods of reference 15. With the exception of takeoff performance, the data are based on standard atmospheric conditions. However, since the engine operating parameters required for noise analysis are sensitive to ambient-temperature variation, the takeoff data were computed for standard day +10 C (18° F). The data indicate that at takeoff velocities and altitudes, the primary and fan nozzles are operating subcritically; that is, the fully expanded exhaust-flow areas are equal to the respective nozzle throat areas.

The inlet recovery corrections presented in figure 34 are based on the geometry of an inlet employed in the study documented in reference 16. Although the inlet was originally designed for a cruise Mach number of 0.98, it was selected for the present study since it exhibits a relatively high pressure recovery of 0.994 at the cruise Mach numbers considered herein. It was assumed that the inlet mass flow is equal to that required by the engine throughout the flight envelope; hence, performance was not penalized for inlet-spillage drag. Engine performance penalties for service airbleed are shown in figure 35. Power extraction for electrical and hydraulic systems was held constant at 48.5 kw (65.0 HP). It was assumed that the nozzle efficiencies of the scaled and reference engines are of equal magnitude; therefore, no performance penalties were assessed for nozzles.

The characteristics of the scaled engine were obtained using the methods of reference 17. Specific fuel consumption, exhaust-gas mass flow, and fully expanded exhaust-gas area were adjusted for the effects of relative-thrust ratio (ratio of required installed thrust to production engine installed thrust). The effects of relative-thrust ratio on fan rotational velocity, and engine mass and dimensions are shown in figure 36. The mass of the scaled engine is 5,527 kg (12,186 lbm), including manufacturer-furnished standard equipment. This mass does not include the inlet, fan cowling, nozzles, or engine-driven

airframe accessories. The installed performance data for the climb and cruise modes are presented in figures 37-41. Data for the takeoff mode are shown in figures 42-49.

The nacelle incorporates a full-length fan duct, and coplanar primary and fan nozzles. The inlet length is equal to the maximum inlet diameter. The nozzle lengths are equal to 1.5 times the primary nozzle diameter. The maximum nacelle diameter is equal to the maximum inlet diameter plus 40.6 cm (16.0 in) for engine-driven accessories and nacelle ventilation. The nacelle external dimensions are presented in Table V.

MISSION ANALYSIS

The design-mission critera specify that the aircraft shall be capable of transporting a 272,155 kg (600,000 lbm) payload a minimum distance of 5,926 km (3,200 n.mi.) at a cruise Mach number of at least 0.7, and shall require a runway length no greater than 3,658 m (12,000 ft). As previously mentioned, the engine selected for the study is a scaled JT9D-7 turbofan. The purpose of the mission analysis is to optimize the required thrust and to obtain the required fuel weights and gross weights, as well as to determine the performance. All performance characteristics are based on standard atmospheric conditions, with takeoff and landing data calculated for sea-level altitude.

Performance Criteria

The criteria employed in determining the various performance parameters are:

Takeoff.- The takeoff distance, based on Federal Aviation Regulations Part 25, is defined as the greater of either 1.15 times the all-engine takeoff distance or the balanced field length with one engine inoperative. Fuel allowance is based on a ten-minute taxi and a one-minute takeoff power setting.

Acceleration-Climb.- A constant equivalent airspeed shall be maintained until the cruise Mach number is reached.

Cruise.- A cruise climb shall be performed at optimum altitude unless constrained by the service ceiling. ·

Reserve Fuel.- The total mission fuel shall include the reserves recommended by the Air Transport Association for international flights, consisting of allowances for:

- Increased trip time of 10 percent.

- Missed approach, followed by acceleration to ·climb velocity.

- Flight to alternate airport, 370 km (200 n.mi.) distance.

- Hold for 30 minutes at 457 m (1,500 ft) altitude.

Method of Analysis

The takeoff and landing performance data were generated with the use of computer programs developed by the Vought Corporation, Hampton Technical Center. Mission performance was evaluated with the use of the mission analysis computer program developed at the Langley Research Center.

Performance Characteristics

Preliminary estimates indicated that because of the relatively low wing loading, engine size is determined by cruise ceiling rather than takeoff field length. In order to determine the design-mission engine size and fuel weight, several iterations of the mission-performance calculations were required. The final results, presented in figure 50, show the effects of installed thrust on takeoff field length and design-mission range. These data are based on a mission-fuel weight of 169,644 kg (374,000 lbm). The selected scale represents an engine which generates a sea-level standard-day installed takeoff thrust of 240,204 N (54,000 lbf). The corresponding design-mission range is 5,954 km (3,215 n.mi.). The takeoff field length at maximum gross weight with 20 degrees of flap deflection is 2,499 m (8,200 ft), which is considerably less than the specified maximum allowable field length.

The effect of engine size on operating empty weight and gross weight are shown in figures 51 and 52, respectively.

Takeoff rotation is initiated at a velocity of 252 km/hr (136 kts). Lift-off is accomplished at 5.5 degrees angle of attack and a velocity of 282 km/hr (152 kts). Optimum climb velocity was determined to be compatible with an equivalent airspeed of 519 km/hr (280 kts).

The effects of cruise Mach number on the design-mission lift-drag ratio and range are shown in figure 53. A reduction in Mach number to 0.68 results in an increase in mission range to 6,543 km (3,533 n.mi.), which is 10 percent greater than that for a cruise Mach number of 0.75.

The effects of gross weight on approach velocity and landing distance for a flap setting of 20 degrees are presented in figure 54. The approach employs a 3-degree glide slope. The relatively high approach velocity is determined by the roll-response capability of the aircraft. The spoilers assist in braking during the ground roll. The landing distance for the design-mission landing weight is 3,018 m (9,900 ft). For the design-mission takeoff gross weight, the equivalent distance is 3,200 m (10,500 ft).

A summary of the design-mission performance characteristics is presented in Table VI. Of particular interest is the design-mission fuel efficiency, which is estimated to be 11.72 ton-km/kg (3.16 ton-n.mi./lbm) of fuel burned. This value is approximately 50 percent greater than that of the most advanced, currently operational, large freighter aircraft.

NOISE

The engine and airframe noise characteristics of the study airplane during takeoff
and approach were estimated at the measurement points (ref. 18) shown in figure 55.
The methods employed and the results are discussed in the following sections.

Method of Analysis

Engine Noise.- The noise characteristics of the fan and jet were evaluated
separately, then combined to determine the overall engine-noise level. The
fan-noise characteristics were determined according to the method of reference 19,
which predicts the variation of fan sound-pressure level, SPL, at a source radius
of 46 m (150 ft). Frequency and directivity angle are treated as functions of fan
performance factors. This technique assumes that a fraction of the mechanical
work is converted into output sound power; hence, both the total-temperature rise
and mass flow of the fan were used in determining the fan source noise. Fan noise
is also affected by the design and operating Mach numbers of the rotor tips, the
number of stator vanes, the blade-passing frequency, and the rotor-stator spacing
ratio. The blade-passing frequency is the product of the number of fan blades
and fan revolutions per second. The rotor-stator spacing ratio is the average
axial distance between the rotor blades and stator vanes divided by the average
rotor-blade axial length. Table VII lists typical input parameters used to
predict the fan-source-noise sound pressure level for each engine. It should
be noted that the fan total-temperature rise, mass flow, and rpm are dependent
on engine performance, which varies during the takeoff mode.

The jet-noise characteristics of the engines were predicted using the coannular-
and single-jet methods of reference 20, which predict the variation of jet-noise
sound pressure level with frequency and directivity angle at a source radius of
46 m (150 ft). The magnitude of the jet noise is dependent on aircraft velocity
and the flow characteristics of each jet, including exit area and velocity, mass
flow, total-temperature ratio, and density. Typical input parameters for pre-
dicting coannular jet noise are listed in Table VIII.

Following thrust cutback, the mass flow and velocity of the fan exit jet are
considerably greater than those of the primary jet. Therefore, for this segment
of the takeoff mode, the jet noise was determined by applying the single-jet
method to the secondary exit flow. Figure 56 shows the variation of the source
noise sound pressure levels with frequency at a directivity angle of 130 degrees
for both the fan and jet following thrust cutback. As indicated, jet source-
noise is predominant at the lower frequencies, whereas fan source noise is
greater at the higher frequencies. However, at the observer locations, the
jet noise levels are predominant due to atmospheric attenuation of the high-
frequency fan noise.

Before combining the source-noise values of the fan and jet, corrections were
applied to each spectra to account for the wing-shielding effects due to mounting
the engines above the wing. Based on preliminary data correlations by the Pratt
and Whitney Aircraft Group, noise reductions of 3 db were applied to cases

20

wherein the wing interferes with the fan or jet noise-source directivity. For the study airplane, these reductions were applied to the fan source noise at angles greater than 20 degrees relative to the engine inlet axis, and to the jet source noise at angles less than 100 degrees relative to the inlet axis. The resulting levels of fan and jet noise were then added logarithmically to obtain a total engine-noise spectra over the applicable ranges of directivity angles and one-third common-octave band frequencies.

For a given instant during takeoff the engine source noise is extrapolated to the observer location along the directivity angle determined by the observer position relative to the aircraft. The extrapolation method includes the effects of tone, spherical divergence, atmospheric attenuation, multiple engines, and ground reflection. Thus, at each observer station on the ground at a particular instant, there is a perceived noise level generated by the engines. The time-history of the perceived noise level is then integrated to obtain an effective perceived noise level, EPNL, at each observer position.

Airframe Noise.- Reference 21 presents the results of a study in which airframe noise data were correlated for multi-engine commercial and military aircraft with aspect ratios from approximately 7 to 10. As part of the study documented in reference 22, airframe noise was also evaluated for an arrow-planform super-sonic transport configuration having an aspect ratio of approximately 1.9. Since the study airplane has an aspect ratio of 4.53, it was assumed that air-frame noise could be approximated by averaging the values predicted by the reference methods. Figure 57 shows the variation of altitude with velocity for an airframe noise level of 108 db as predicted by the reference methods. The average-value curve represents the estimated noise level of the study airplane.

Predicted Noise Levels

Engine Noise at Takeoff- In order to minimize engine noise at the centerline measurement point (located 6,486 m (3.5 n.mi.) from the break-release point), engine thrust was reduced 5,944 m (19,500 ft) from brake release. The thrust cutback point was determined from the results of a previous study reported in reference 23. To optimize the noise level of the study airplane at the measurement points, the takeoff profile was varied to evaluate the effect of cutback altitude on the engine effective perceived noise level (EPNL) at both the sideline and centerline measurement points. Figure 58 indicates that as altitude is increased engine sideline noise increases and centerline engine noise decreases. Figure 58 also exhibits a decrease in the overall airframe sound pressure level (OASPL) at the centerline measurement point as thrust cutback altitude is increased. It will be noted that airframe OASPL is approximately 5 dB greater than the centerline engine EPNL. Since OASPL is an instantaneous sound pressure level rather than a time-history value, it should be reduced slightly to correlate with the EPNL; however, the amount of reduction is less than 4 dB. Consequently, the most significant noise source of the study airplane is that of the airframe.

It was determined that at a cutback distance of 5,944 m (19,500 ft), the maximum allowable altitude is 515 m (1,691 ft), because aircraft acceleration capability is inadequate to attain higher altitudes. To reach this maximum altitude, the required all-engine takeoff field length is 2,248 m (7,375 ft). After thrust cutback, the climb gradient was decreased to 4 percent in accordance with regulations of reference 18. The takeoff profile and two measurement points (ref. 18) are shown in figure 59. The lift-off velocity is 287 km/hr (155 kts). At the point-1 measurement station, the velocity is 321 km/hr (173 kts), the lift coefficient is 0.75 and the lift-drag ratio is 19.1.

The variations of EPNL along the runway centerline and along the sideline (649 m (0.35 n.mi.) from the centerline) are shown in figures 60 and 61, respectively. Figure 60 exhibits an airframe OASPL of 94.8 dB at the 6,486 m (3.5 n.mi.) centerline measurement point. Therefore, without engine cutback, engine EPNL would exceed the airframe noise. Contour plots for engine ENPL values of 90 dB and 100 dB are presented in figure 62.

Engine Noise During Approach.- During approach, the engines operate at idle thrust and have a considerably lower noise level than the airframe. Figure 55 shows the 3-degree approach profile and the reference 18 measurement point which is located 1,853 m (1.0 n.mi.) from the 15.2 m (50.0 ft) threshold point. The aircraft landing weight is 479,719 kg (1,057,600 lbm) and the landing velocity is 300 km/hr (162 kts). For a 3-degree approach profile, the altitude at the 1,853 m (1.0 n.mi.) point is 112 m (369 ft). These values were employed in the airframe noise calculations.

Airframe Noise.- The airframe OASPL of the study aircraft was computed by averaging the values generated by the methods of references 21 and 22. The input values and the corresponding OASPL values from each method at the 2 runway centerline measurement points are presented in Table IX. As shown, the values of airframe OASPL at the measurement points during takeoff and approach are 94.78 dB and 104.77 dB, respectively.

CONCLUSIONS

A preliminary design study has been conducted of a large span-distributed loading cargo aircraft capable of transporting a 272,155 kg (600,000 lbm) payload of large containers over intercontinental distances. The conclusions are as follows:

1. The specifications for payload weight, density, and dimensions in essence configure the wing and establish the low wing loading of only about 342 kg/m^2 (70 lbm/ft^2).

2. The structural weight comprises only about 18 percent of the design maximum gross weight, exemplifying the magnitude of structural efficiency achievable through the utilization of the span-distributed loading concept. However, weight reduction is limited since neither weight nor the external

loads are uniformly distributed along the span. Also, the extreme depth of the spars is not as advantageous as might be expected since the failure modes occur in buckling with very low maximum allowable stress.

3. Although the geometric aspect ratio is 4.53, the winglet effect of the wing-tip-mounted vertical tails provides an effective aspect ratio of 7.9.

4. At the cruise Mach number of 0.75, the optimum lift-drag ratio is 19.0. The lift drag ratio achieved with the maximum Breguet range factor is 18.65.

5. In cruising flight, the trim-drag penalties can be large for a tailless aircraft with winglets. In this design, these penalties are negated by controlling the center of gravity by fuel management so as to maintain zero elevon angle.

6. Controls-fixed longitudinal dynamic analyses for the takeoff and approach modes indicate that the current Hardened Stability Augmentation System (HSAS) two-second minimum limit to double amplitude imposes restrictions on the rearward center-of-gravity travel which preclude the use of optimum elevon settings. Therefore, efficient operation of the aircraft in these flight modes would require the development of a faster-reacting control system.

7. Sufficient control power to handle the large rolling moment of inertia dictates a relatively high minimum approach velocity of 315 km/hr (170 kts).

8. The airplane has acceptable spiral and Dutch-roll modes and a marginally acceptable roll-damping mode. The roll-mode time constant is acceptable for maximum gross weight, but is slightly large for the reserve-fuel gross weight.

9. An attempt to improve aerodynamic efficiency by the employment of camber was abandoned due to the requirement for a c.g. location too far forward.

10. The engine selected for the study is a scaled JT9D-7 turbofan providing an installed static thrust of 240,200 N (54,000 lbf) per engine at sea-level, standard-atmosphere conditions. Six such engines are required. Because of the relatively low wing loading, engine size is determined by cruise ceiling rather than takeoff field length.

11. The design-mission range at M = 0.75 is 5,954 km (3,215 n.mi.). However, a decrease in Mach number to 0.68 results in a 10-percent increase in range.

12. The FAR-25 takeoff field length at maximum gross weight is 2,499 m (8,200 ft). The landing distance is 3,018 m (9,900 ft) for the design mission landing weight and 3,200 m (10,500 ft) at the design takeoff gross weight.

13. The design-mission fuel efficiency is approximately 50 percent greater than that of the most advanced, currently operational, large freighter aircraft.

14. The most significant noise source of the study airplane is that of the airframe. However, for both takeoff and approach the levels are below the FAR-36 limit of 108 dB.

REFERENCES

1. Whitener, C. P.; Gratzer, B. L.; and Whitlow, D. H.: Technical and Economic Assessment of Span-Distributed Loading Cargo Aircraft Concepts. Boeing Company, NASA CR-144963, 1976.

2. Anon: Technical and Economic Assessment of Span-Distributed Loading Cargo Aircraft Concepts. Douglas Aircraft Company, NASA CR-144962, 1976.

3. Johnston, W. M.; Muehlbauer, J. C.; Eudaily, R. R.; Farmer, B. T.; Honrath, J. F.; and Thompson, S. G.: Technical and Economic Assessment of Span-Distributed Loading Cargo Aircraft Concepts. Lockheed-Georgia Company, NASA CR-145034, 1976.

4. Whitehead, Allen H.: The Promise of Air Cargo - System Aspects and Vehicle Design. NASA TM X-71981, 1976.

5. Bauer, F.; Garabedian, P.; Korn, D.; and Jameson, A.: Supercritical Wing Sections II. Lecture Notes in Economics and Mathematical Systems, M. Beckmann and H. P. Kunzi, eds., Springer-Verlag, 1975.

6. Whitcomb, Richard T.: A Design Approach and Selected Wind-Tunnel Results at High Subsonic Speeds for Wing-Tip Mounted Winglets. NASA TN D-8260, 1976.

7. McGhee, Robert J.; and Beasley, William D.: Low Speed Aerodynamic Characteristics of a 17-Percent-Thick Airfoil Section Designed for General Aviation Applications. NASA TN D-7428, 1973.

8. Goldhammer, M. I.: A Lifting Surface Theory for the Analysis of Nonplanar Lifting Systems. AIAA Paper 76-16, 1976.

9. Brune, E. F.: Analysis and Design of Airplane Structures. Tri-State Offset Company, Cincinnati, Ohio, 1949.

10. Woodward, F. A.: An Improved Method for the Aerodynamic Analysis of Wing-Body-Tail Configurations in Subsonic and Supersonic Flow. NASA CR-2228, 1973.

11. Putnam, Lawrence E.: An Analytical Study of the Effects of Jets Located More Than One Jet Diameter Above a Wing at Subsonic Speeds. NASA TN D-7754, 1974.

12. Abbott, Ira H.; and Von Doenhoff, Albert E.: Theory of Wing Sections, Dover Publications, New York, 1959.

13. Air Force Flight Dynamics Laboratory: Stability and Control Methods. USAF Stability and Control Datcom, 1960, Revised 1975.

14. Anon: Flying Qualities of Piloted Airplanes. Military Specification MIL-F-8785B (ASG), 1969.

15. JT9D Commercial Turbofan Engine Installation Handbook. Pratt & Whitney Aircraft Group, United Technologies Corporation, 1967.

16. General Electric Company: Propulsion System Studies for an Advanced High Subsonic, Long Range Jet Commercial Transport Aircraft, 1972.

17. Anderson, B. A.: Scaling the JT9D Engine. TDM-1990, Revised. Pratt & Whitney Aircraft Group, United Technologies Corporation, 1968.

18. Department of Transportation, Federal Aviation Administration Noise Standards: Aircraft Type and Airworthiness Certification, Federal Aviation Regulations Part 36, 1974.

19. Heidmann, M. F.: Interim Prediction for Fan and Compressor Source Noise. NASA TM X-71763, 1975.

20. Stone, James R.: Interim Prediction Method for Jet Noise. NASA TM X-71618, 1974.

21. Hardin, Jay C.; Fratello, David J.; Hayden, Richard E.; Kadman, Yoran; and Africk, Steven: Prediction of Airframe Noise. NASA TN D-7821, 1975.

22. Baber, Hal T.; and Swanson, E. E.: Advanced Supersonic Technology Concept AST-100 Characteristics Developed in a Baseline-Update Study. NASA TM X-72815, 1976.

23. Vought Corporation, HTC: Advanced Supersonic Technology Concept Study Reference Characteristics. NASA CR-132374, 1973.

TABLE I - GROUP WEIGHT SUMMARY

	kg	lbm
Wing	70385	155173
Vertical Tail	3462	7632
Fuselage	1910	4210
Landing Gear	29472	64975
Nacelle	4774	10524
Structure Total	110003	242514
Engine	32394	71416
Thrust Reversers	4637	10222
Miscellaneous Systems	961	2118
Fuel System-Tanks and Plumbing	5434	11980
Propulsion Total	43425	95736
Surface Controls	7620	16800
Auxiliary Power	435	960
Instruments	1014	2236
Hydraulics	4055	8940
Electrical	3986	8787
Avionics	1024	2257
Furnishings and Equipment	889	1960
Air Conditioning	91	200
Anti-icing	95	210
Systems and Equipment Total	19209	42350
Manufacturing/Certification Tolerance		
Weight Empty	172637	380600
Crew and Baggage (3)	306	675
Loadmaster (1)	102	225
Unusable Fuel	1860	4100
Engine Oil	442	975
Passenger Service	11	25
Operating Weight	175359	386600
Cargo (Gross) Containerized	272155	600000
Zero Fuel Weight	447514	986600
Mission Fuel	169644	374000
Design Gross Weight	617158	1360600

TABLE II - MASS DATA SUMMARY

		MAX TAKE-OFF GROSS WT			RES. FUEL GROSS WT.	
MASS, kg		617158			479719	
lbm		1360600			1057600	
CONDITION		CRUISE	LANDING	TAKE-OFF	CRUISE	LANDING
HORIZONTAL c.g. Location	m	29.8	30.1	30.1	29.8	30.3
	ft	97.7	98.6	98.9	97.7	99.5
	percent $\bar{c}$	29.0	30.4	30.9	29.0	31.8
ROLL INERTIA, I_x, kg-m^2(10^6)		315	316	318	284	285
slug-ft^2(10^6)		232	233	234	209	210
PITCH INTERTIA, I_y, kg-m^2(10^6)		50	49	49	53	48
slug-ft^2(10^6)		37	36	36	39	35
YAW INERTIA, I_z, kg-m^2(10^6)		352	350	349	320	314
slug-ft^2(10^6)		259	258	257	236	231
PRODUCT OF INERTIA, J_{xz}, kg-m^2(10^6)		1.6	1.5	1.1	0.9	1.2
slug-ft^2(10^6)		1.2	1.1	0.8	0.7	0.9
PRINCIPAL AXIS ANGLE	Rad.	.044	.041	.039	.025	.044
OF INCLINATION	Deg.	2.52	2.35	2.23	1.43	2.52

TABLE III. - FUEL DISTRIBUTION

Point	c.g. % c̄	Design Gross Weight	Total Fuel	Fuselage Tank	Wing Fwd Tanks	Wing Aft Tanks
1	15.0	617158 (1360600)	169644 (374000)	32205 (71000)	137438 (303000)	0 (0)
2	29.0	617158 (1360600)	169644 (374000)	0 (0)	61870 (136400)	107774 (237600)
3	30.4	617158 (1360600	169644 (374000)	0 (0)	48611 (107168)	121033 (266832)
4	30.9	617158 (1360600	169644 (374000)	0 (0)	43875 (96728)	125768 (277272)
5	35.5	617158 (1360600	169644 (374000)	0 (0)	0 (0)	169644 (374000)
6	29.0	479719 (1057600)	32205 (71000)	32205 (71000)	0 (0)	0 (0)
7	5.6	345002 (760600)	169644 (374000)	32205 (71000)	137438 (303000)	0 (0)
8	37.4	345002 (760600)	169644 (374000)	0 (0)	0 (0)	169644 (374000)
9	23.0	207564 (457600)	32205 (71000)	32205 (71000)	0 (0)	0 (0)
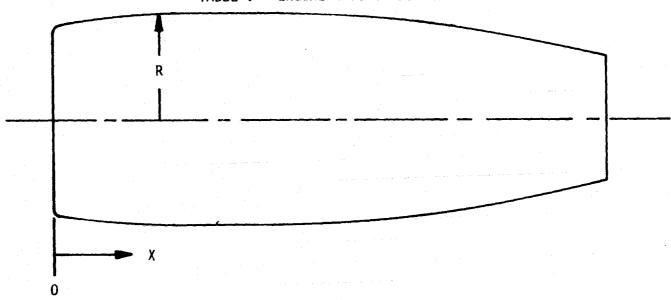
Weights shown in kilograms
with pounds in parenthesis

TABLE IV - LATERAL-DIRECTIONAL DYNAMIC CHARACTERISTICS

STABILITY MODE	DUTCH-ROLL			ROLL	SPIRAL
Symbols	ζ_{min}	$(\zeta\omega_n)_{min}$ RAD/SEC	$\omega_{n,min}$ RAD/SEC	t_{max} SEC	$t_{2_{min}}$ SEC
Requirements	.08	.5	.4	1.4	20
Inherent MLW	0.285	0.168	0.590	1.367	-40.60 *
characteristics RLW	0.301	0.171	0.570	1.405	-42.27

* Negative sign denotes the time to half the amplitude of oscillation (spirally stable)

TABLE V - ENGINE NACELLE DIMENSIONS

X		R		X		R	
m	in	m	in	m	in	m	in
0	0	1.267	49.9	4.521	178	1.585	62.4
.025	1	1.311	51.6	5.080	200	1.577	62.1
.127	5	1.367	53.8	5.588	220	1.557	61.3
.254	10	1.415	55.7	6.096	240	1.519	59.8
.508	20	1.478	58.2	6.604	260	1.466	57.7
.762	30	1.514	59.6	7.112	280	1.405	55.3
1.016	40	1.539	60.6	7.620	300	1.328	52.3
1.524	60	1.567	61.7	8.128	320	1.224	48.2
2.032	80	1.580	62.2	8.509	335	1.113	43.8
2.769	109	1.585	62.4	8.738	344	1.016	40.0

TABLE VI - MISSION PERFORMANCE

MISSION: Design (M = .75)

MODEL: FLYING WING SPANLOADED CARGO AIRCRAFT

AIRCRAFT CHARACTERISTICS

Take-Off gross weight	- kg (1bm)	617158	(1360600)
Operating weight empty	- kg (1bm)	175359	(386600)
Payload (gross)	- kg (1bm)	272155	(600000)
Wing area	- m² (ft²)	1724	(18560)
S.L. Static Thrust per Engine (std day)			
Uninstalled	N (1bf)	262445	(59000)
Installed	N (1bf)	240204	(54000)
Take-off installed thrust to weight ratio		.238	
Take-off wing loading - kg/m² (1bm/ft²)		357.9	(73.3)

Design Mission

	OPERATING WEIGHTS, kg (1bm)		Δ FUEL kg (1bm)		Δ RANGE km (n.m.)		Δ TIME MIN
Take-off	617158	(1360600)					
			2540	(5600)	0		11
Start Climb	614618	(1355000)					
			16021	(35320)	370	(200)	31
Start Cruise	598597	(1319680)					
			116573	(257000)	5213	(2815)	387
End Cruise	482024	(1062680)					
			2291	(5050)	370	(200)	20
End Descent	479733	(1057630)					
Taxi-in			816	(1800)	0		5
Block fuel and Time			138241	(304770)			454
Trip Range					5953	(3215)	

NOTES: 1. Taxi-in fuel taken out of reserves at destination

2. C.A.B. range corresponding to block time and fuel equals trip range minus traffic allowances for maneuver, traffic and airway distance.

TABLE VI - MISSION PERFORMANCE - Concluded

MODEL: FLYING WING SPANLOADED CARGO AIRCRAFT

Reserve Fuel Breakdown, kg (1bm)

1.	10% trip time	11657	(25700)
2.	Missed Approach	1814	(4000)
3.	370 km (200 n. mi.) to alternate airport	11839	(26100)
4.	30 min. holding at 457 m. (1500 ft.)	6908	(15230)
	Total Reserve	32219	(71030)

Initial Cruise Conditions:

Lift Coefficient	.3323	
Drag Coefficient	.01782	
Lift/Drag	18.65	
TSFC, kg/hr/N (1bm/hr/1bf)	.0637	(.625)
Altitude, m (ft)	10119	(33200)

Fuel Efficiency:

Ton Kilometers per kg of Fuel Burned = 11.72

(Ton Nautical Miles per Pound of Fuel Burned = 3.16)

TABLE VII - TYPICAL INPUT PARAMETERS FOR PREDICTING TAKE-OFF FAN NOISE

Diameter (D) - m (ft)	2.643	(8.671)
Fan total temperature rise - C(°F)	86.06	(154.9)
Mass flow - kg/sec (slugs/sec)	763.35	(52.315)
Number of fan blades	108	
Number of Stator Vanes	46	
Rotor tip Mach number at design	1.287	
Rotor stator spacing ratio	1.267	
Fan rotor speed (ω) - rpm	2972	

Calculated Values

Blade passing frequency $(F_b) = \dfrac{NB \ast \omega}{60}$ (Hz)   5350

Rotor tip operating Mach Number $(M_{TR}) = \dfrac{\pi D \ast \omega}{60 \ast c_a}$ 1.2127

TABLE VIII - TYPICAL INPUT PARAMETERS FOR PREDICTING TAKE-OFF JET NOISE

Primary Exit Flow Characteristics

Area - m^2 (ft^2)	0.8393	(9.04)
Mass flow - kg/sec (slug/sec)	157.72	(10.809)
Velocity - m/s (fps)	369.65	(1212.75)
*Density - kg/m^3 ($slug/ft^3$)	0.5081	(0.00099)
Total temperature ratio = $T_{T,jet} / T_{T,a}$	2.66	

Fan Exit Flow Characteristics

Area - m^2 (ft^2)	2.3950	(25.78)
Mass flow - kg/sec (slug/sec)	763.35	(52.315)
Velocity - m/s (fps)	286.91	(941.32)
*Density - kg/m^3 ($slug/ft^3$)	1.1109	(.00216)
Total Temperature ratio - $T_{T,jet}/T_{T,a}$	1.15	

Aircraft Velocity - m/s (fps)   88.40   (290.03)

* Density is computed from the Mass flow, velocity and jet exit area.

TABLE IX - INPUT PARAMETERS FOR AIRFRAME NOISE DURING TAKE-OFF AND APPROACH

Parameter	Take-off		Approach	
Aircraft Weight - W kg (lbm)	617158	(1360600)	479719	(1057600)
Wing Span - b m (ft)	88.39	(290)	88.39	(290)
Aspect Ratio A	4.531		4.531	
Altitude - h m (ft)	542.90	(1781.2)	112.36	(368.64)
Velocity - V m/s (kts)	89.30	(173.4)	83.39	(162.0)
Wing Area - S m² (ft²)	1724.28	(18560)	1724.28	(18560)
Equation 1 Airframe OASPL - dB	98.37		109.24	
Equation 2 Airframe OASPL - dB	91.19		100.29	
*Spanloader Airframe OASPL - dB	94.78		104.77	

$$*OASPL_{spanloader} = 1/2 \; (\text{Equation 1 OASPL} + \text{Equation 2 OASPL})$$

$$OASPL_{airframe} = 10 \, Log_{10} \left[\frac{V^{3.34} W^{0.60} b^{0.63}}{h^{1.83} A^{3.03}} \right] + 56.14 \qquad (1)$$

$$OASPL = 10 \, Log_{10} \left[\frac{V^{3.17} W^{0.88}}{h^{1.62} S^{0.16} A^{2.06}} \right] + 41.29 \qquad (2)$$

NOTE: DIMENSIONS SHOWN IN METERS WITH FEET
IN PARENTHESES EXCEPT AS NOTED

.524 RAD.
(30.000 DEG.)

.061 RAD.
(3.500 DEG.)

19.507
MAC (64.000)

REAR BEAM .629C

ELEVON HINGE LINE .80C

FRONT BEAM .124C

44.196
(145.000)

22.098
(75.200)

20.178
(66.200)

13.519
(44.350)

LINE .85C

HINGE

HINGE

SPOILER

FLAP

(2.500)

.209 RAD.
(2.000 DEG.)

₵ AIRCRAFT

S	172 m²
	(1856.0 ft²)
S_v	110 m²
	(1181 ft²)
THRUST/ENGINE	240204 N
	(54000 lb)
TOGW	617158 kg
	(1360600 lb)

11.372
(37.309)

11.227
(36.800)

19.812
(65.000)

DIHEDRAL .052 DEG.
(3.000 DEG.)

RUDDER HINGE LINE .80C

19.610
(64.334)

14.360
(48.000)

34.240
(112.334)

22.921
(75.200)

.218 RAD.
(3.000 DEG.)

STATIC
GROUND LINE

3.588
(11.772)

29.012
(95.185)

33.905
(111.238)

56.025
(185.025)

Figure 1. - Span-distributed-load cargo airplane configuration.

FRONT REAM

REAR BEAM

FUEL TANKS
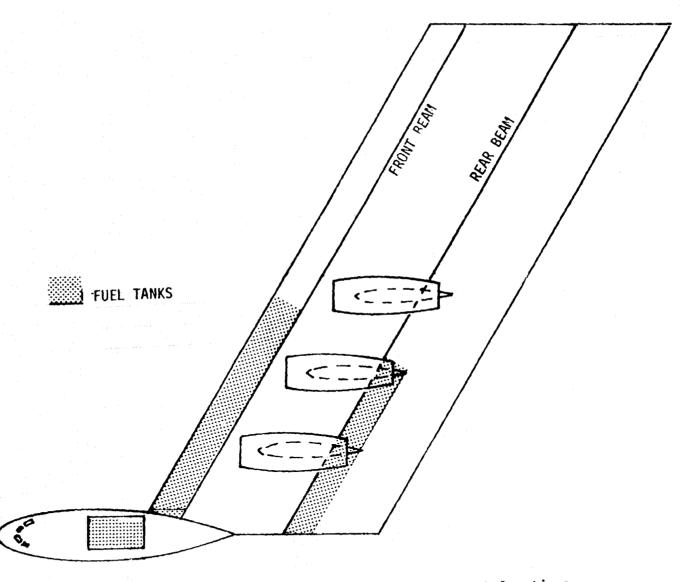
Figure 2. - Schematic of fuel tank locations.
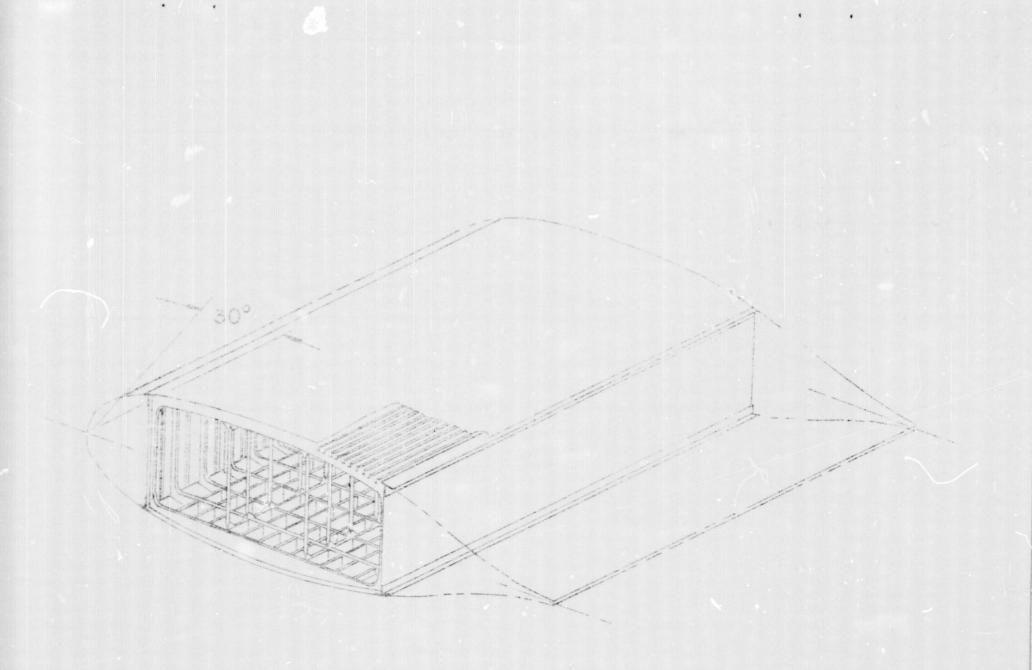
Figure 3. - Schematic of wing-box structural concept.

0.124C   0.377C   0.629C

0.850C
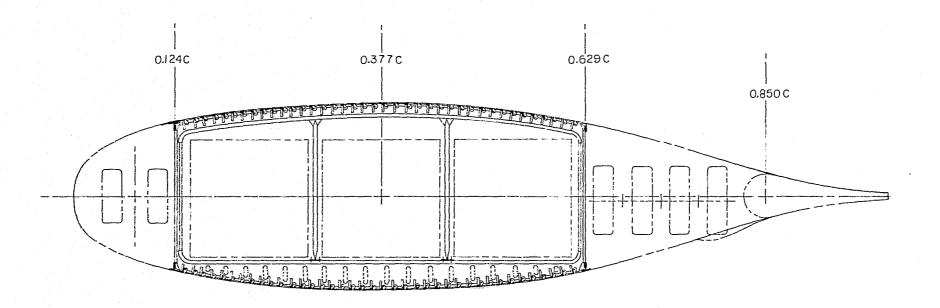
Figure 4. - Cross section of wing normal to the leading edge.
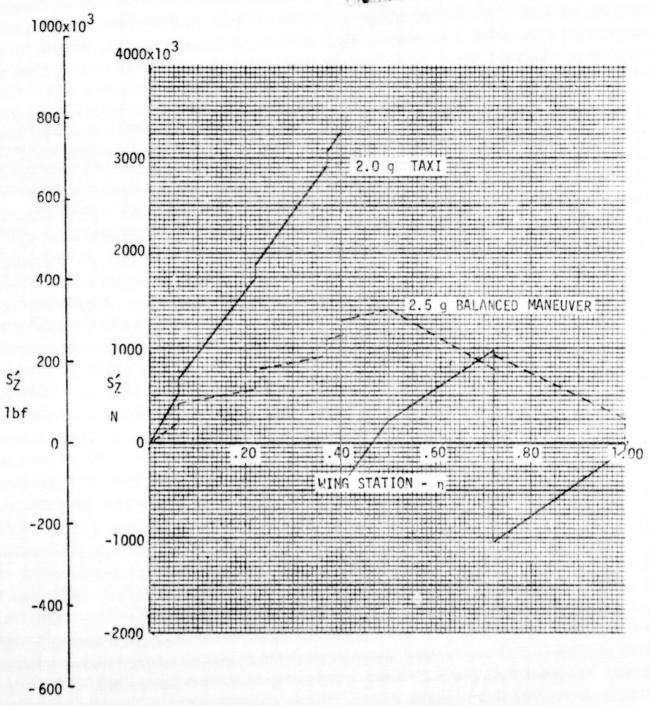
Figure 5. - Net limit swept axis shears.
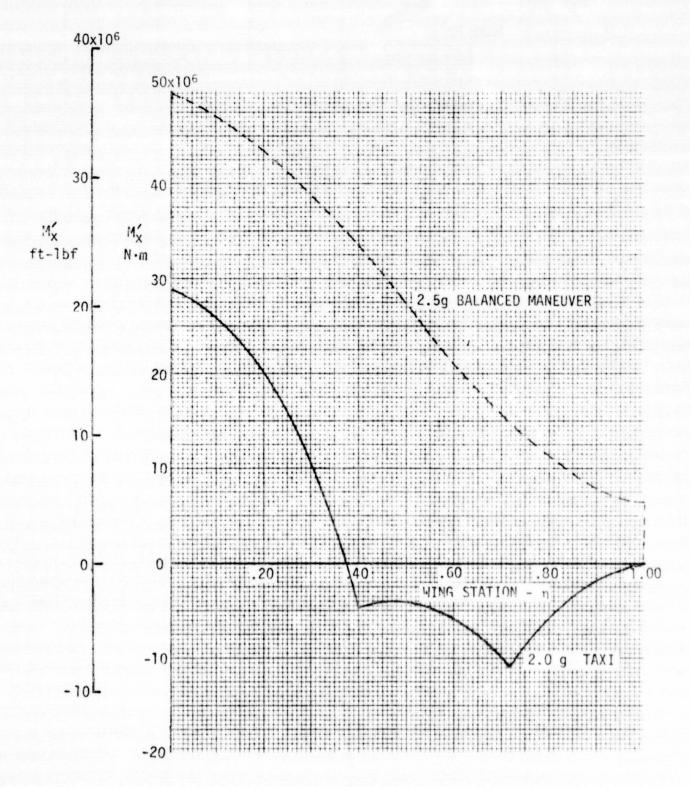
Figure 6. - Net limit swept axis bending moments.
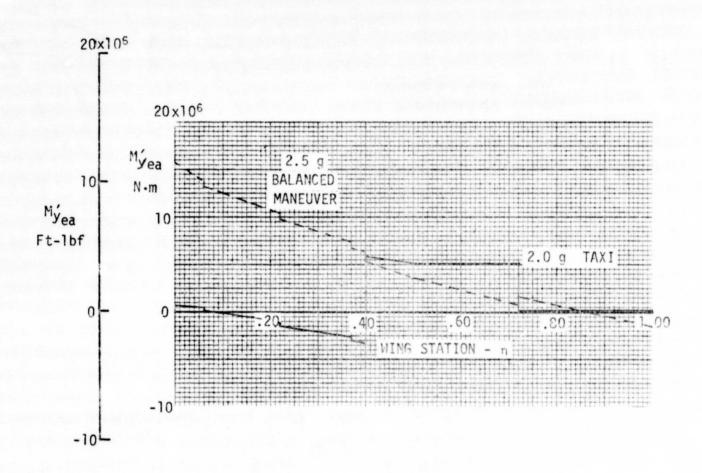
Figure 7. - Net limit swept axis torsions.

WING STATION 51.036 m
167.44 ft

OUTBOARD LANDING
GEAR POSITION

$\eta = .86$

AFT. BEAM .629C

$\eta = .71$

FRONT BEAM .124C

$\eta = .43$
$\eta = .39$
$\eta = .37$

$\eta = .26$

INBOARD LANDING
GEAR POSITION

$\eta = .13$

$\eta = 0$

WING STATION 0.00
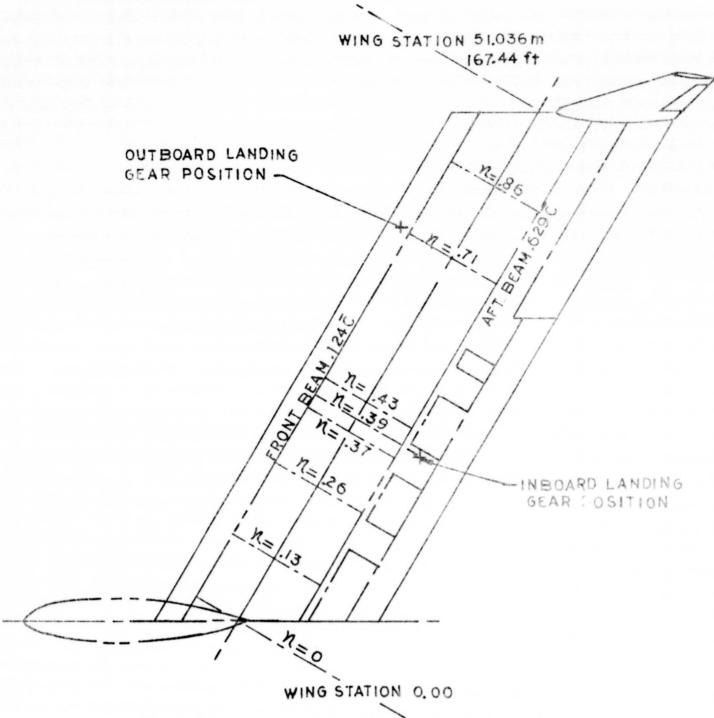
Figure 8. - Semispan stations at which wing-box loads were analyzed.

$$q_{web} = q_v + q_s$$

$$V_{web} = q_{web} (h_{web})$$
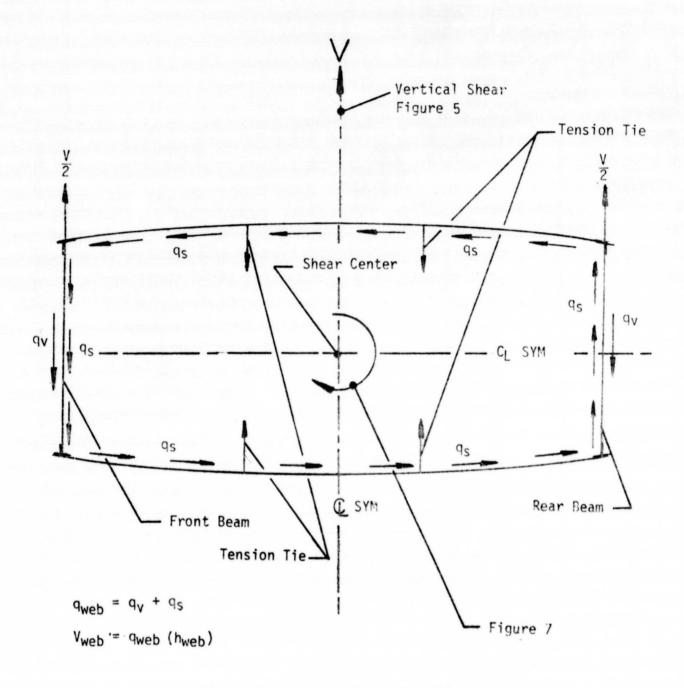
Figure 9. - Shear flow schematic.
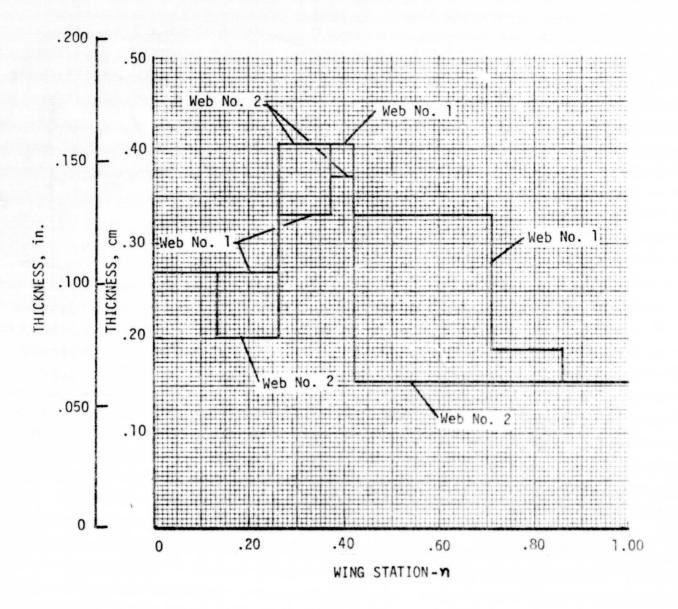
Figure 10. - Web thickness of beam
No. 1 and beam No. 2
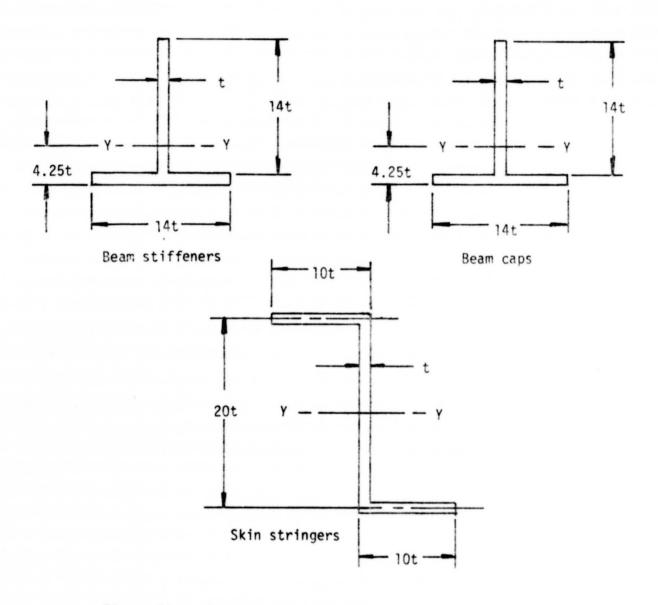
Figure 11. - Cross-sections of beam stiffeners and caps, and skin stringers.
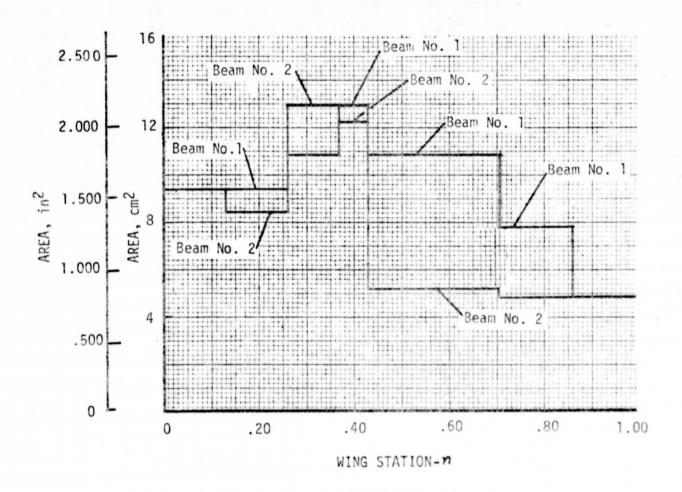
Figure 12. - Stiffener sectional areas of
beam No. 1 and beam No. 2.
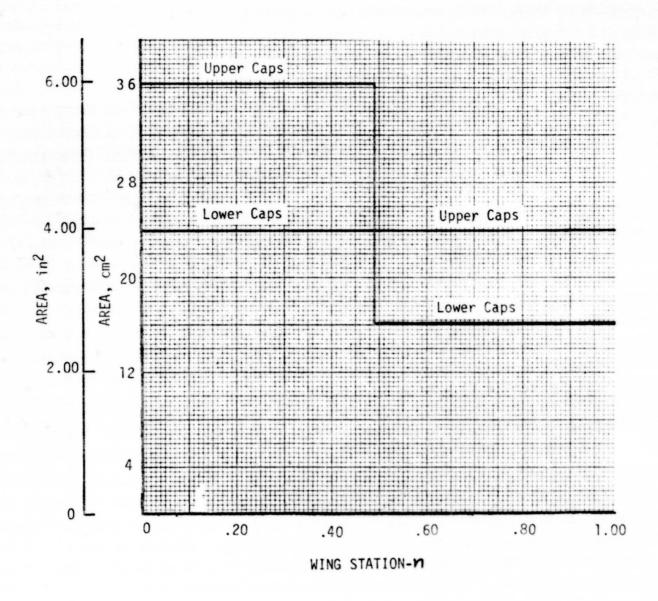
Figure 13. - Upper and lower beam cap sectional areas
beam No. 1 and beam No. 2.
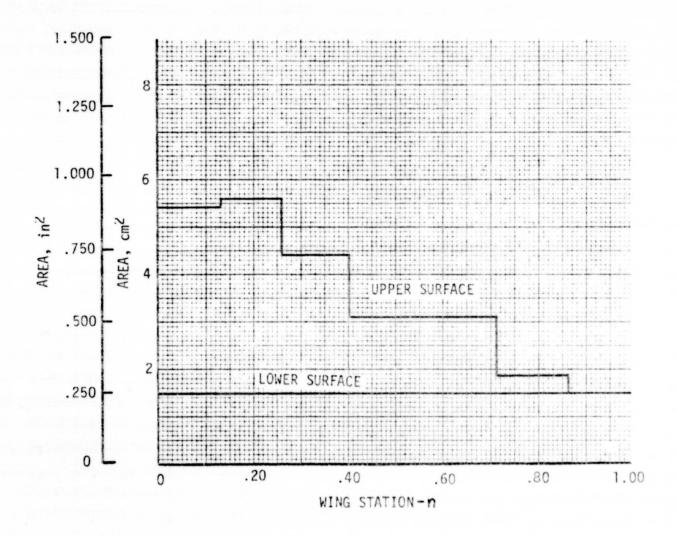
Figure 14. - Wing box stringer sectional areas,
upper and lower surfaces.
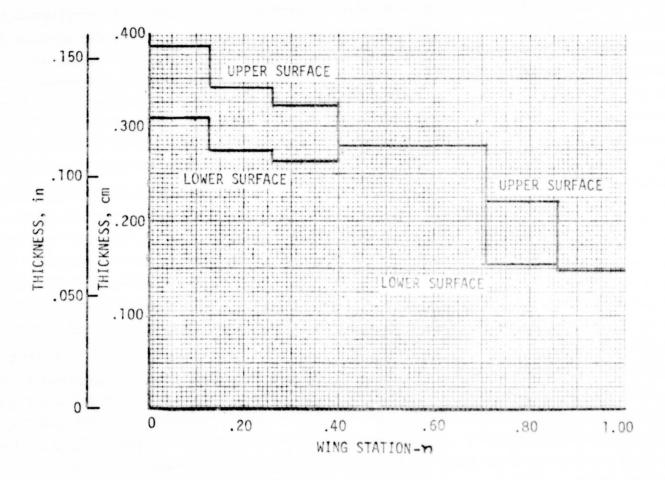
Figure 15. - Wing box skin thickness,
upper and lower surfaces.
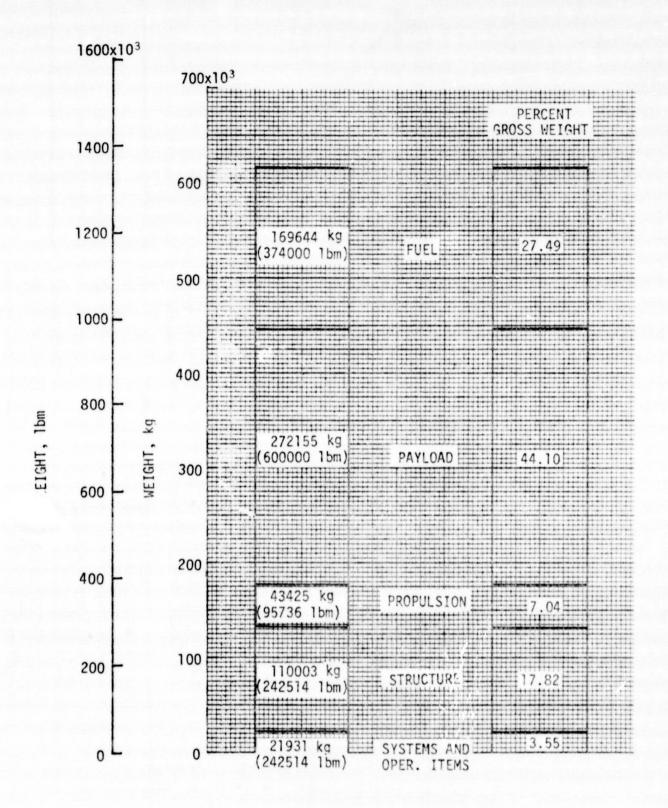
Figure 16. - Gross weight breakdown.
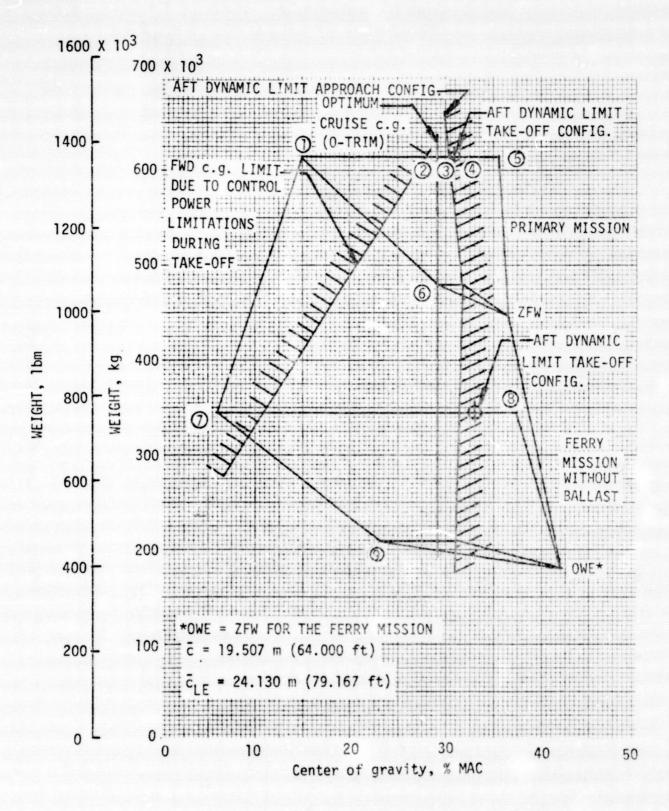
Figure 17. - Loadability envelope with flight limitations.
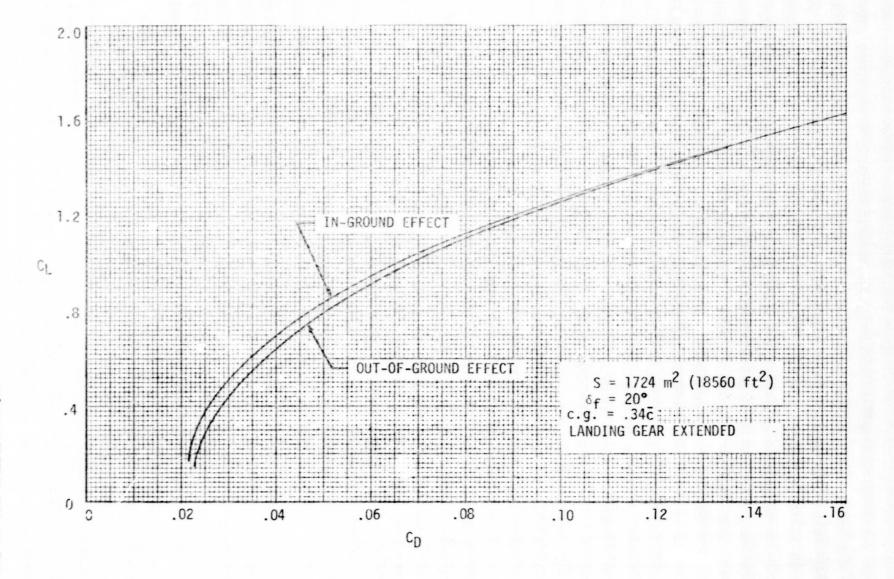
Figure 18. - Landing lift-drag polar.
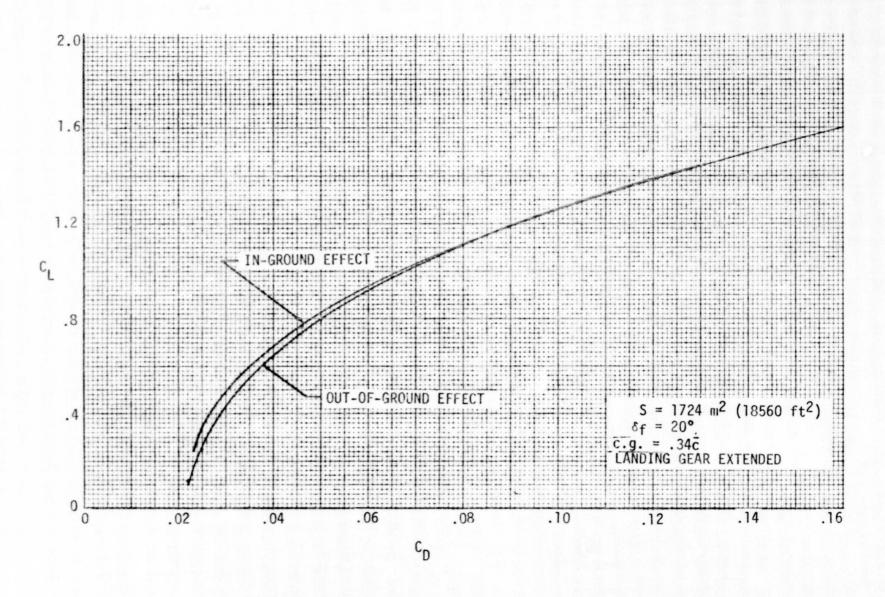
Figure 19. - Take-off lift-drag polar.
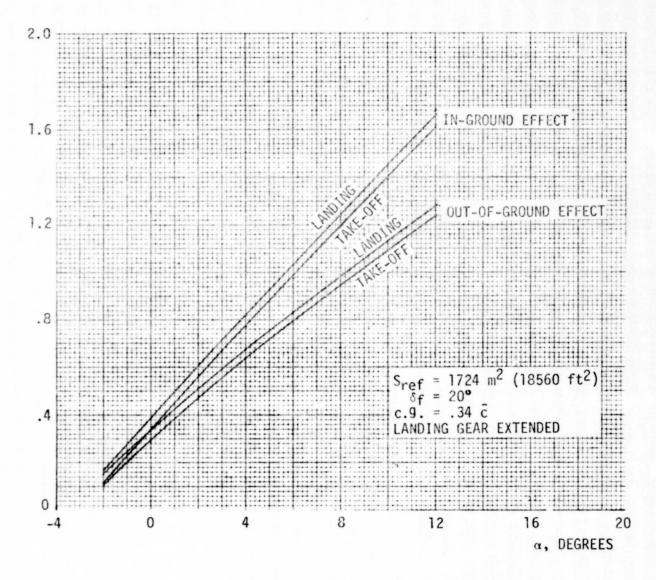
Figure 20. - Lift coefficient variation with angle of attack for take-off and landing.
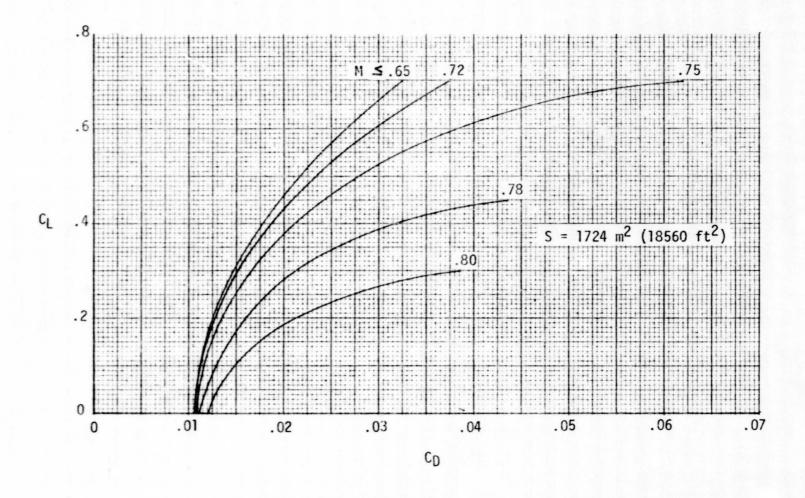
Figure 21. - Cruise lift-drag polars.
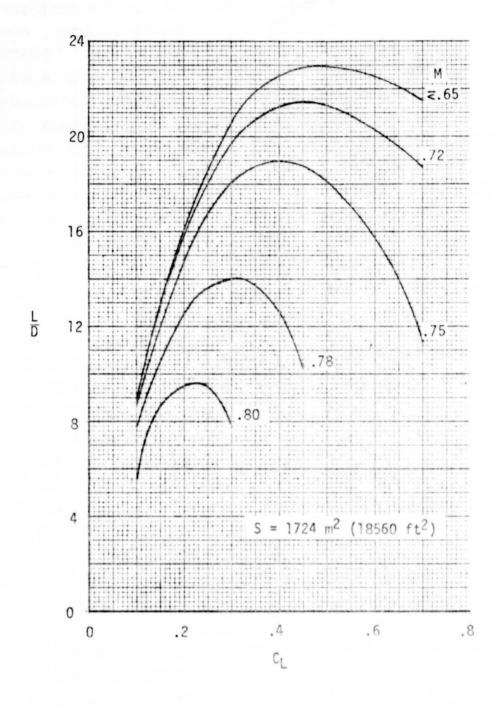
Figure 22. - Lift-drag variation with lift coefficient
for several cruise Mach numbers.
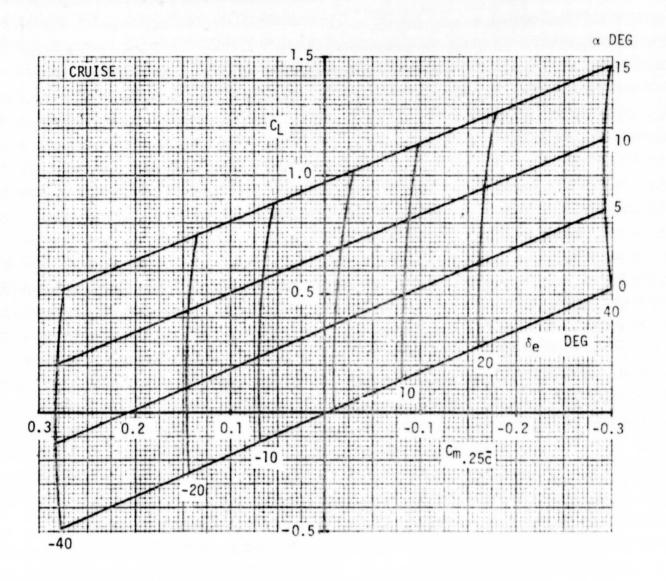
Figure 23. - Effect of elevon deflection on lift and pitching moment, δf = 0 DEG.
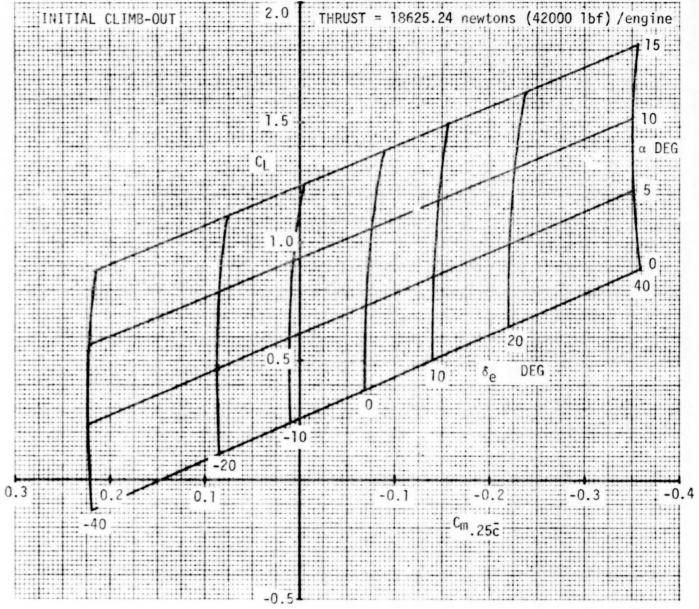
Figure 24. - Effect of elevon deflection on lift and pitching moment, δ_f = 20 DEG.
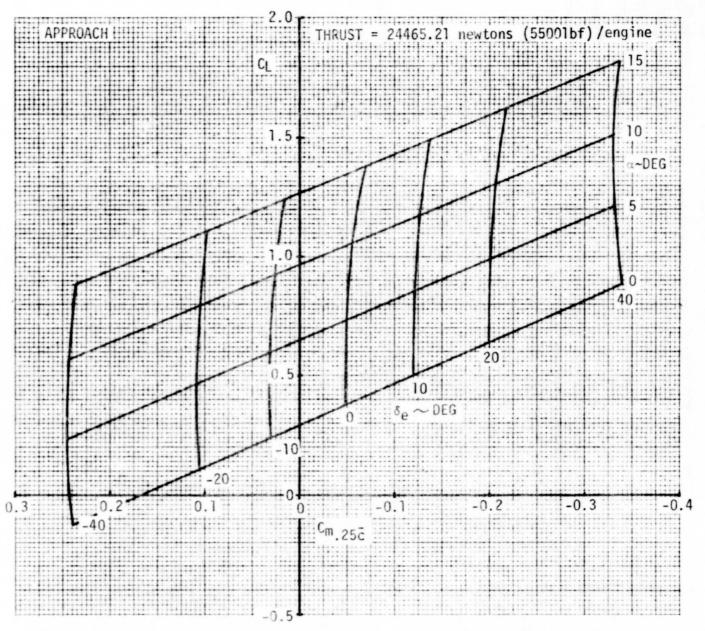
Figure 25.- Effect of elevon deflection on lift and pitching moment, δ_f = 20 DEG.
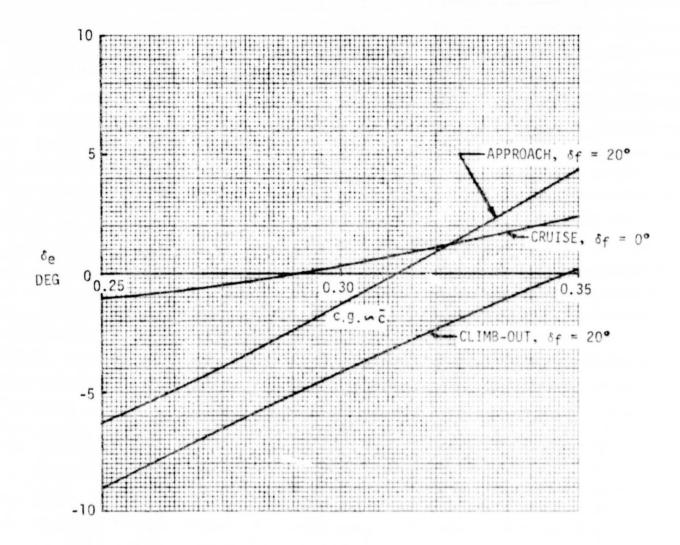
Figure 26.- Elevon required to trim.
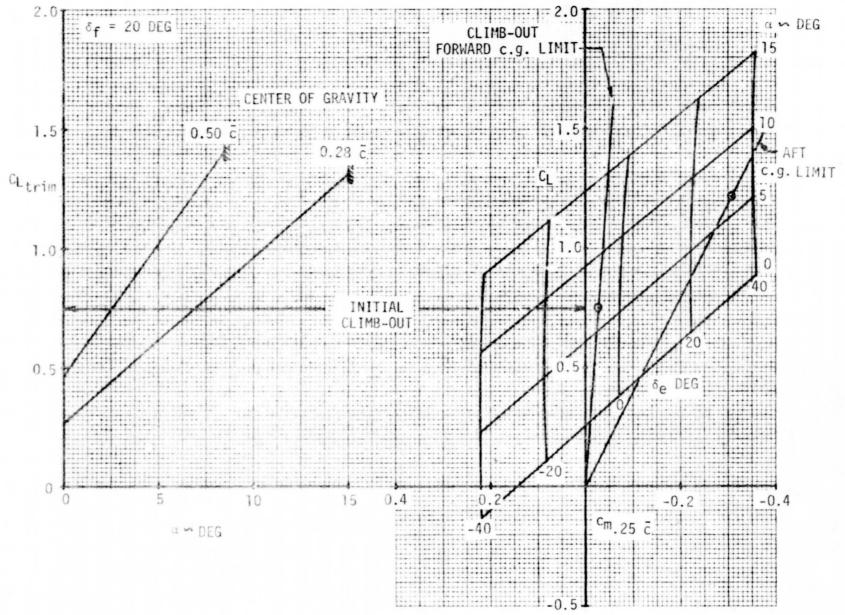
Figure 27.- Spanloader initial climb-out trim and stability, out of ground effect.
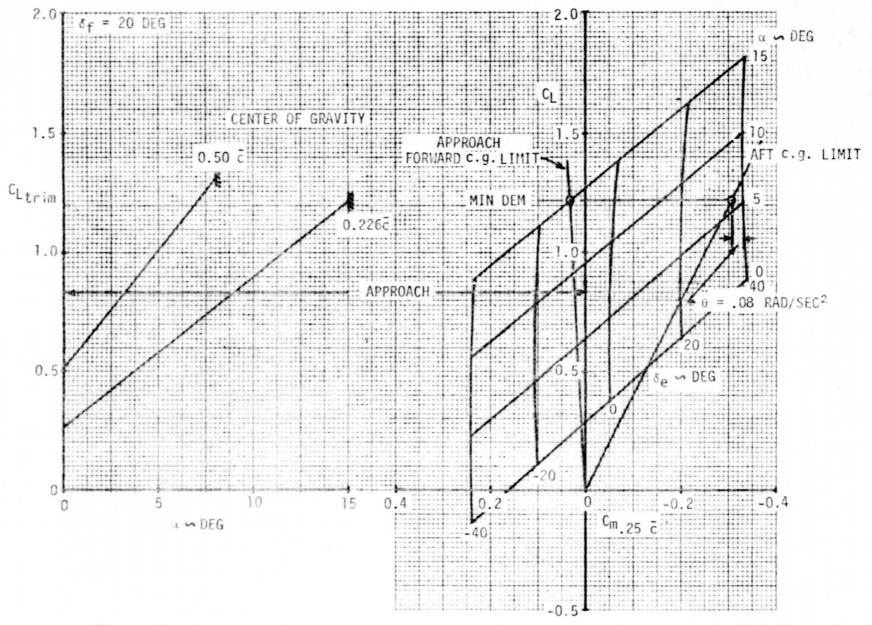
Figure 28. - Aircraft final approach trim and stability, out of ground effect.
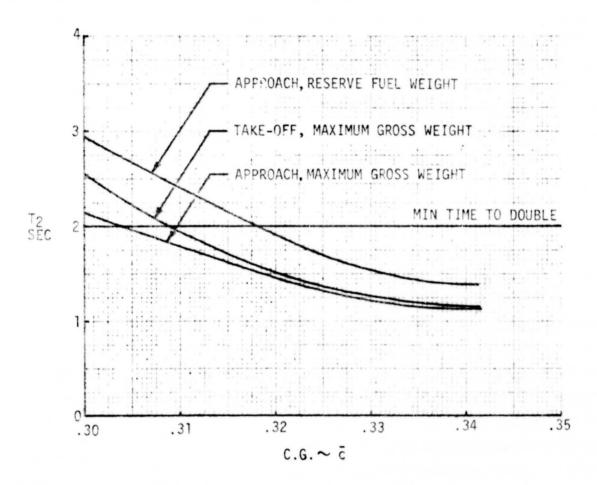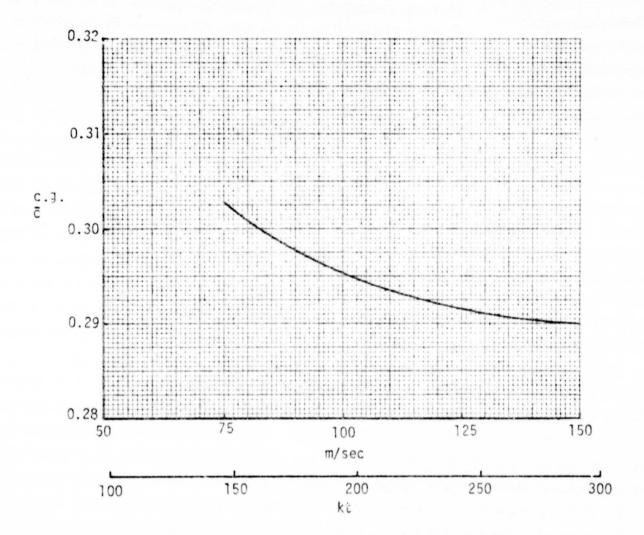
Figure 29. - Estimated time to double amplitude for the aircraft in the approach and take-off configurations

EQUIVALENT AIRSPEED

Figure 30. - Rearward dynamic center-of-gravity limit for
climb-acceleration mode, δf = 0 DEG.

W = 617158 KG (1360600 LBM), MAXIMUM THRUST ON FIVE OPERATING ENGINES

V = 263 km/hr (142 KT) EAS

S_{vt} = 219.4 m^2 (2362 ft^2)
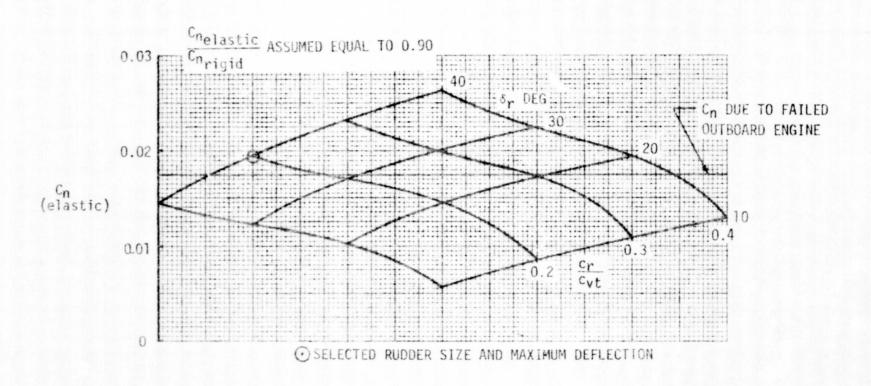
Figure 31. — Estimated aircraft directional control capability assuming an outboard engine failure.

APPROACH CONFIGURATION

$\dfrac{C_{n_{elastic}}}{C_{n_{rigid}}}$ ASSUMED EQUAL TO 0.90

CLASS III, CATEGORY C, REF 14
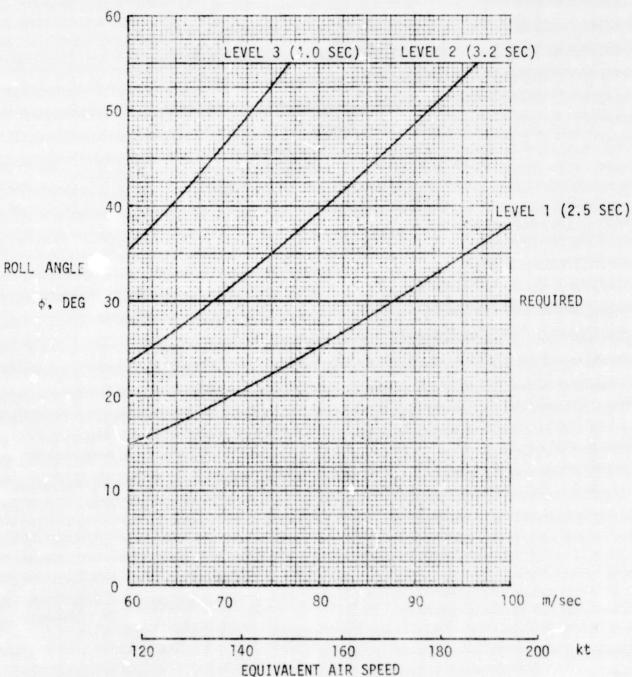
Figure 32.- Estimated aircraft roll response to a
lateral step input, landing-approach

$V_{CW} = 56$ km/hr (30 kt)
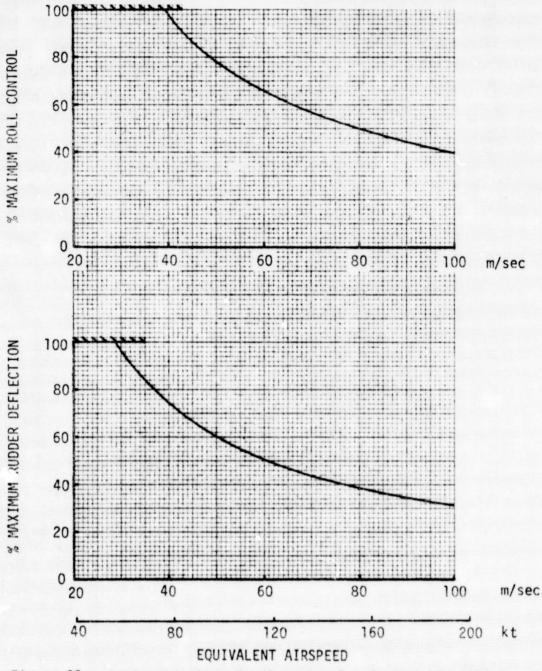
Figure 33.- Estimated aircraft directional trim requirements in a 90 degree cross-wind.
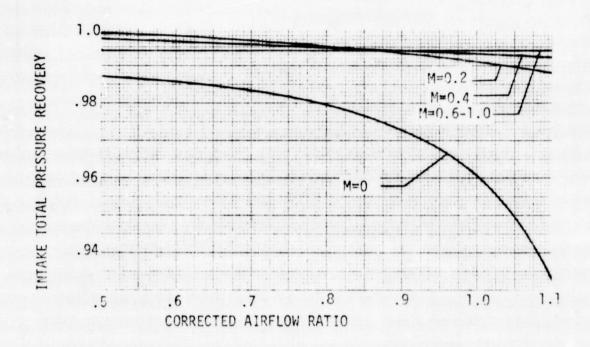
Figure 34. - Air-inlet total pressure recovery.
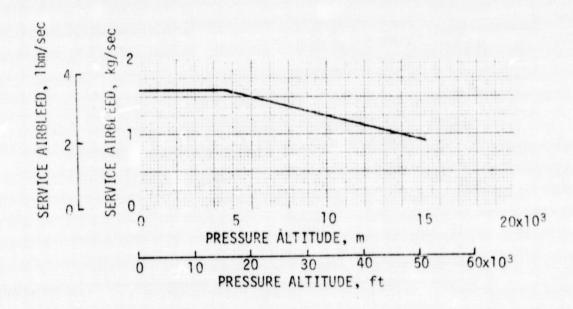
Figure 35. - Service airbleed schedule per engine.

Figure 36. - Engine and nacelle scaling factors
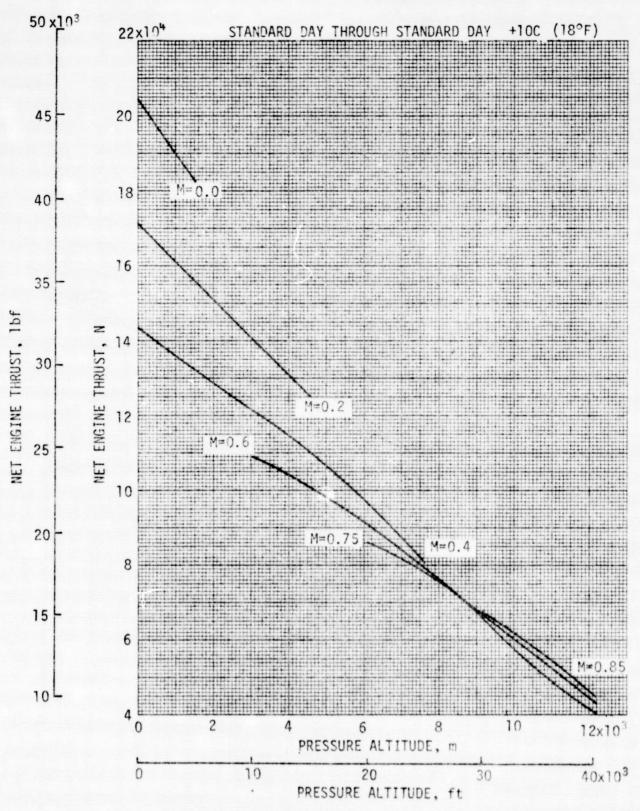
Figure 37. - Installed net engine thrust at maximum climb power.

STANDARD DAY
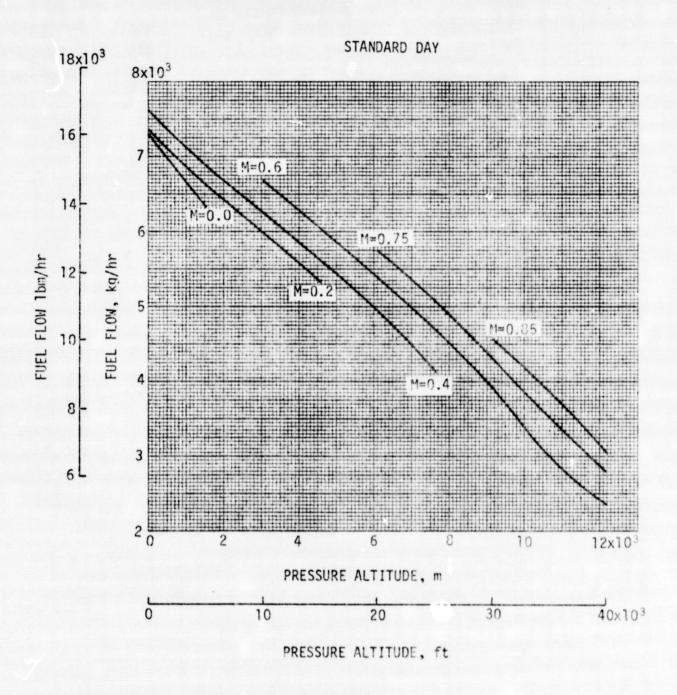
Figure 38. - Installed fuel flow at maximum climb power.
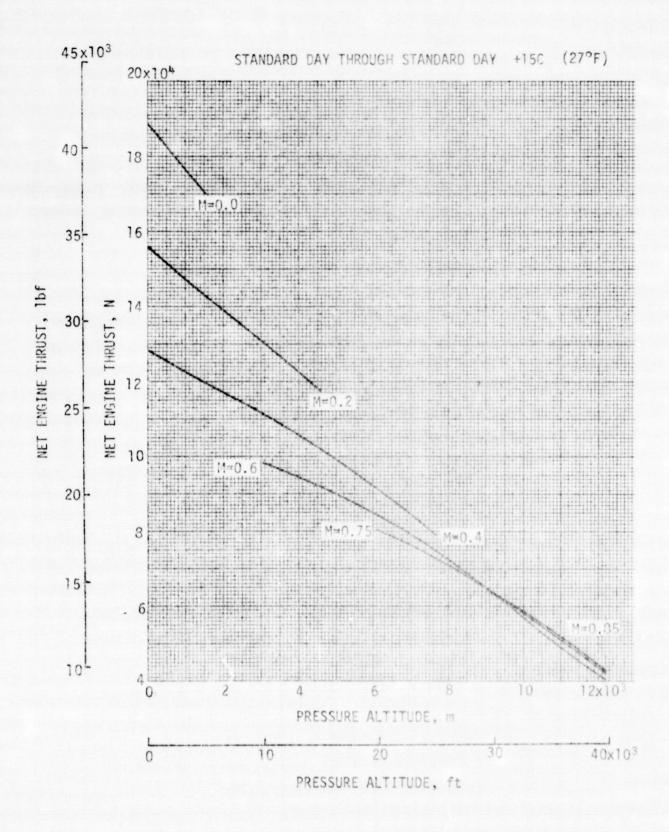
Figure 39. - Installed net engine thrust at maximum cruise power.
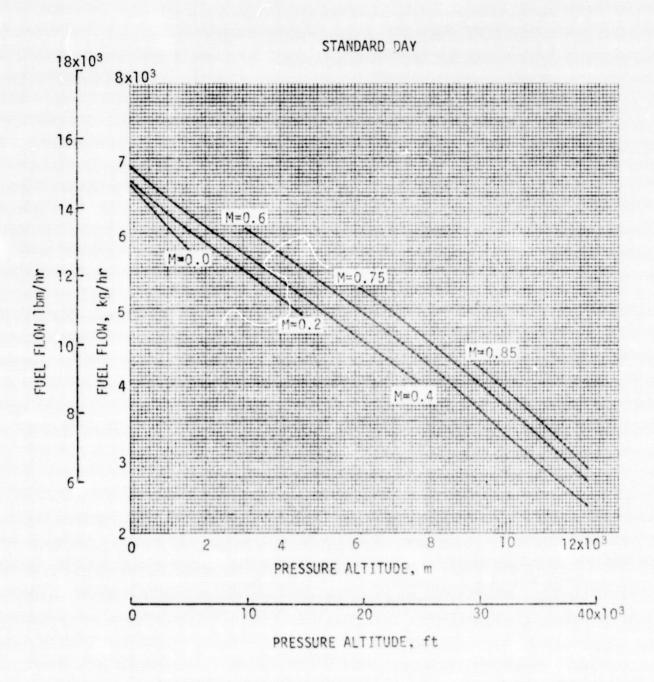
Figure 40. - Installed fuel flow at maximum cruise power.
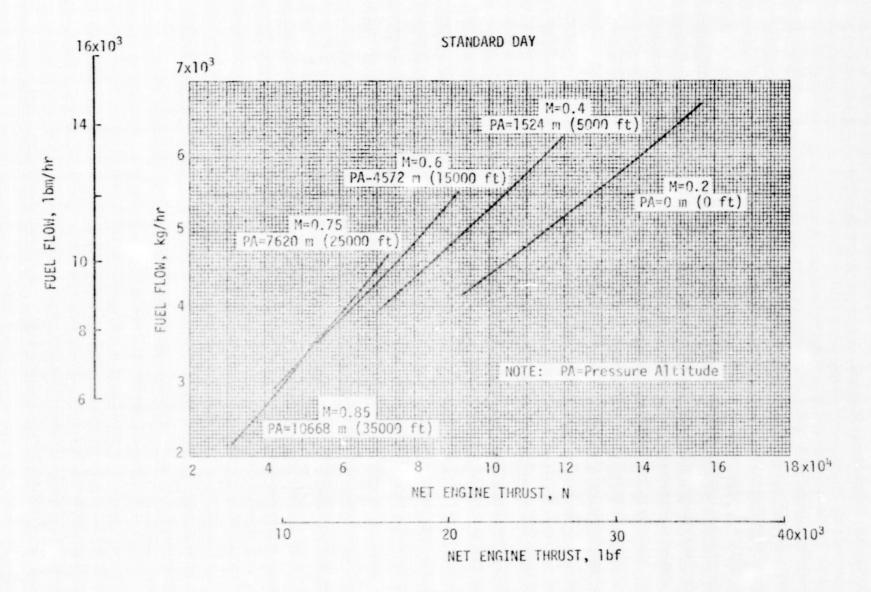
Figure 41. - Installed fuel flow at maximum and part power cruise thrust.
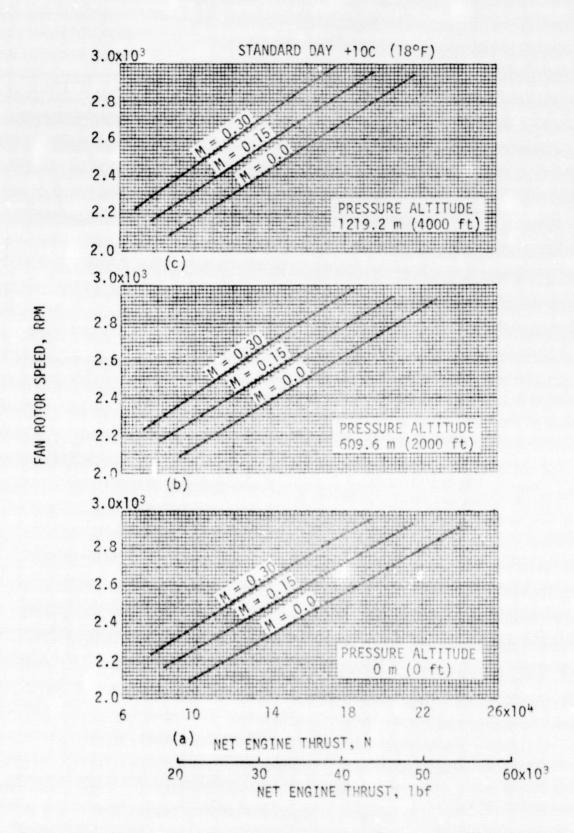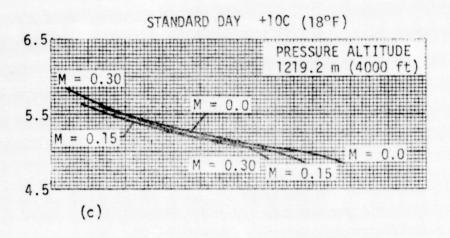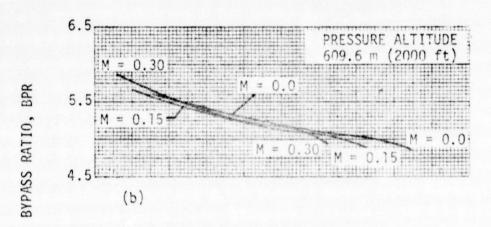
Figure 42. - Installed fan rotor speed at take-off and part power cruise.
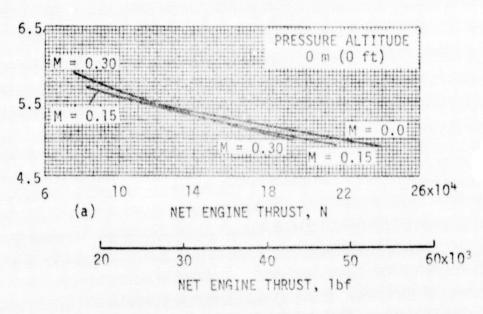
Figure 43. - Installed engine bypass ratio at take-off and part power cruise.
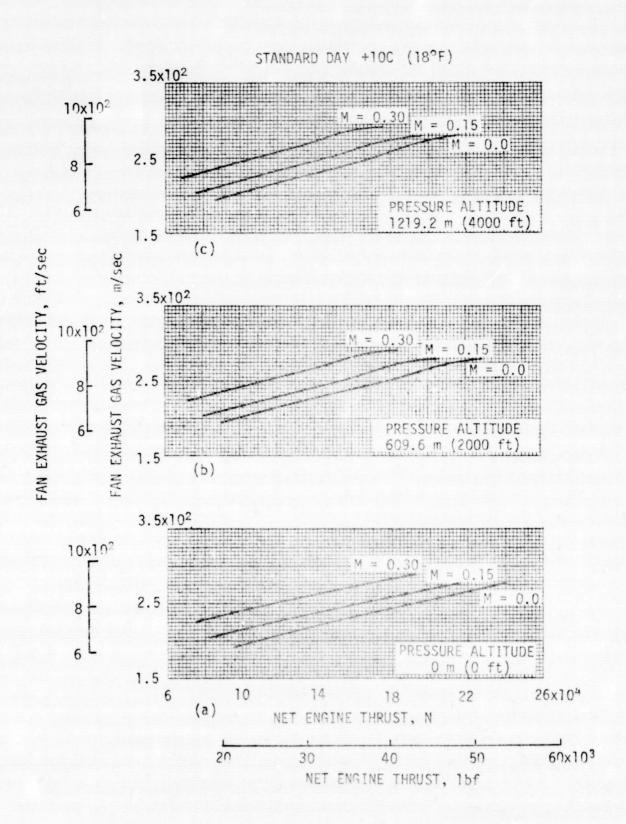
Figure 44.-Installed fan exhaust gas velocity at take-off and part power cruise.
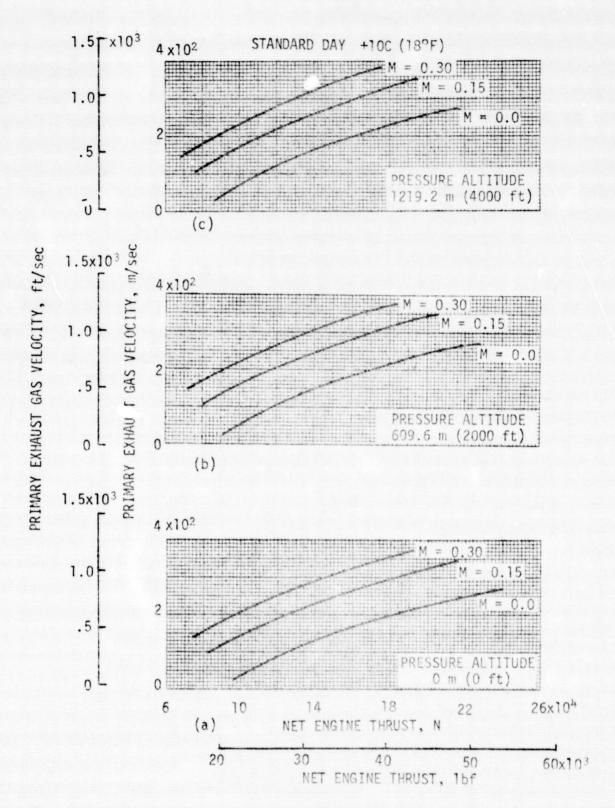
Figure 45. - Installed primary exhaust gas velocity at take-off and part power cruise.
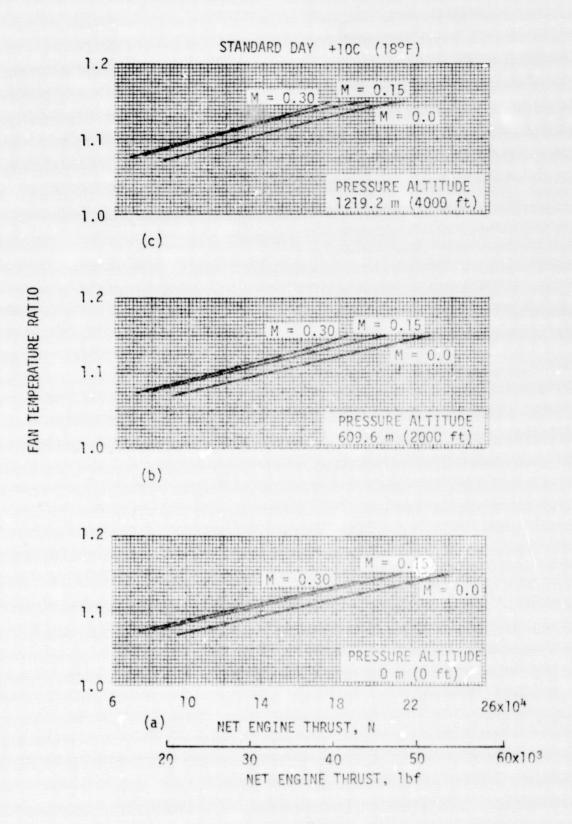
Figure 46. - Installed fan temperature ratio at take-off and part power cruise.

STANDARD DAY +10C (18°F)
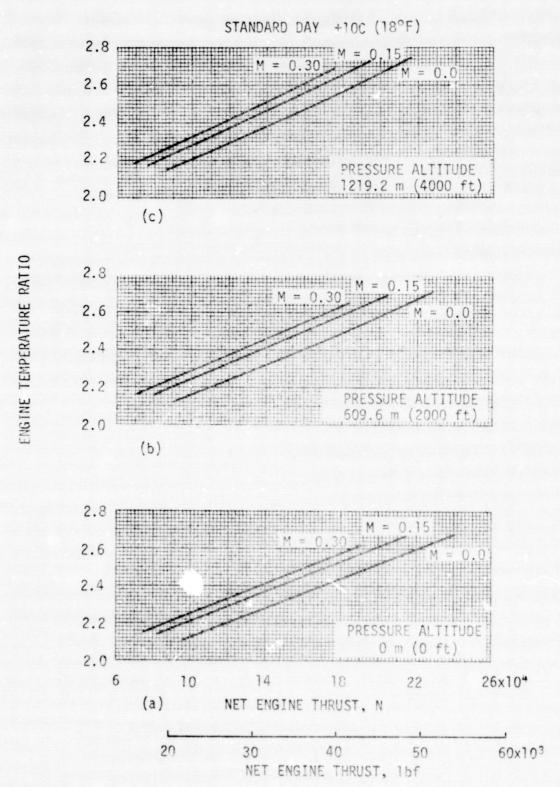
Figure 47. - Installed engine temperature ratio at take-off
and part power cruise.
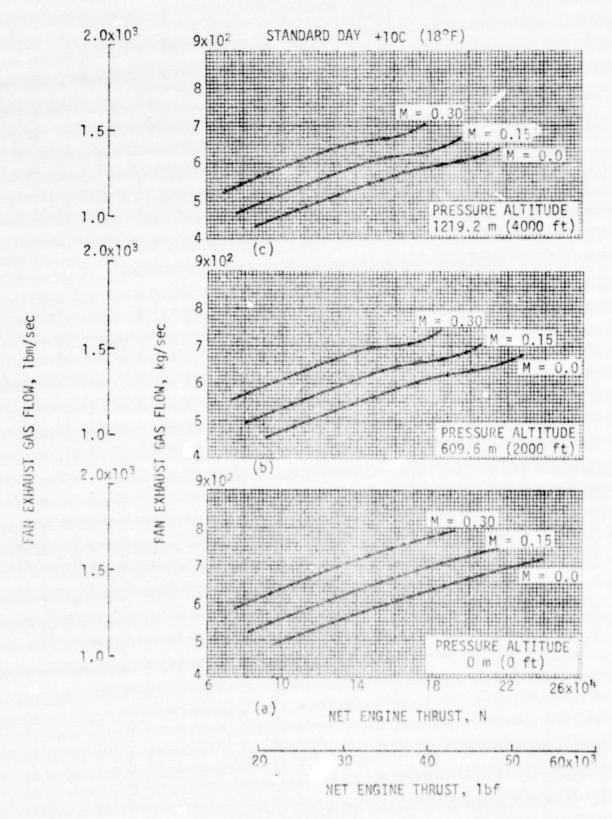
Figure 48. - Installed fan exhaust flow at take-off and part power cruise.
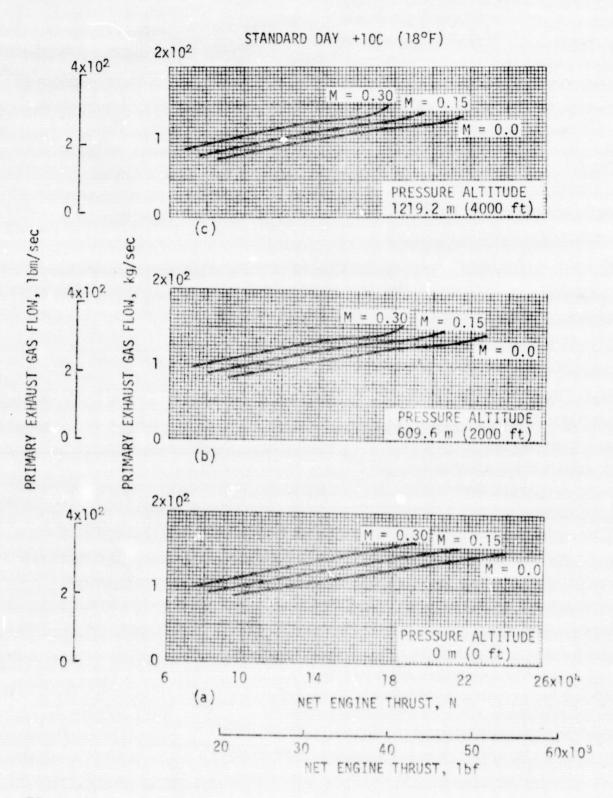
Figure 49. - Installed primary exhaust gas flow at take-off and part power cruise.
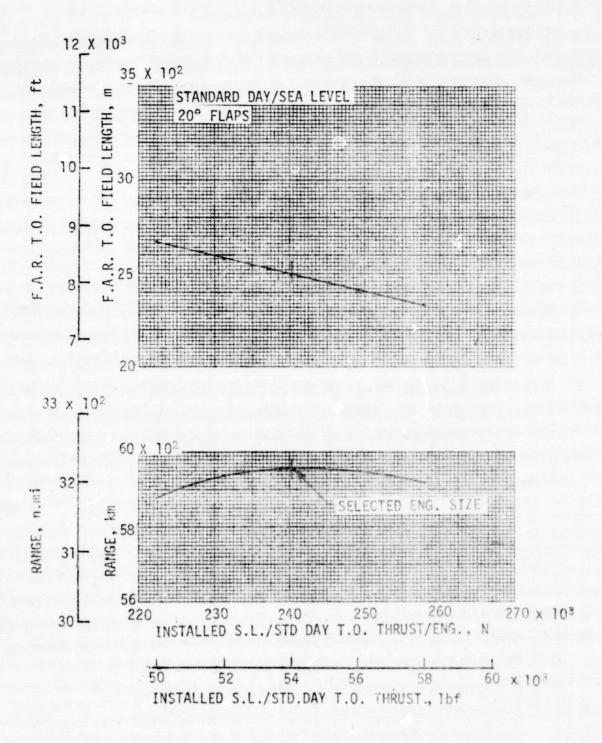
Figure 50. - Effect of engine size on range and FAR take-off field length.
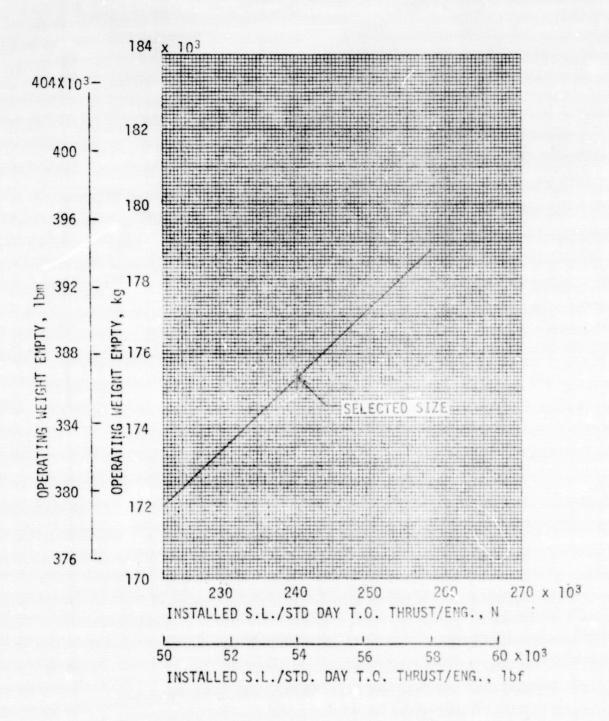
Figure 51. - Effect of engine size on OWE.
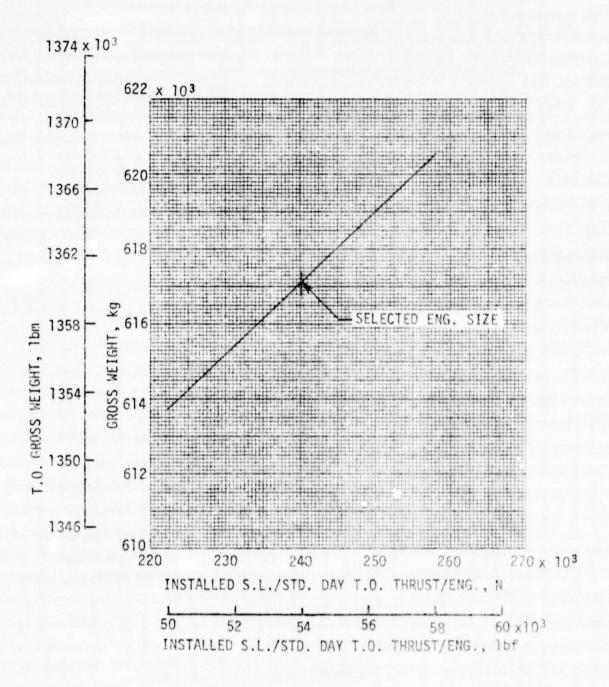
Figure 52. - Effect of engine size on gross weight.
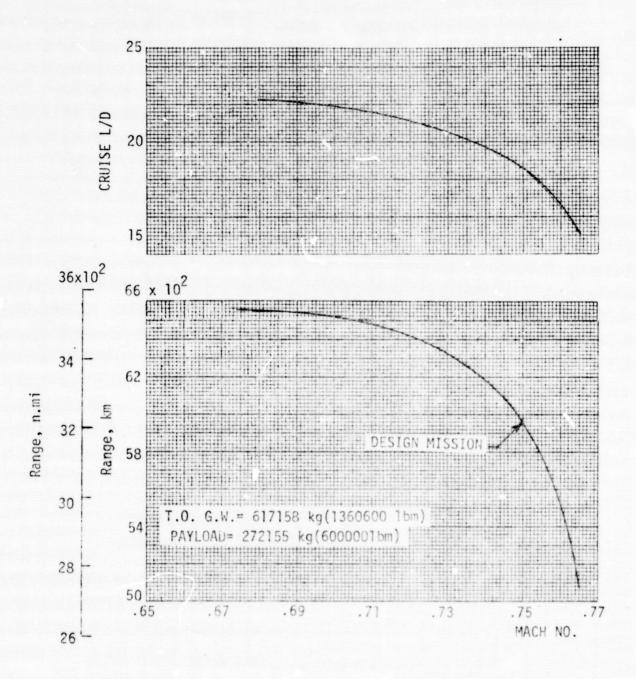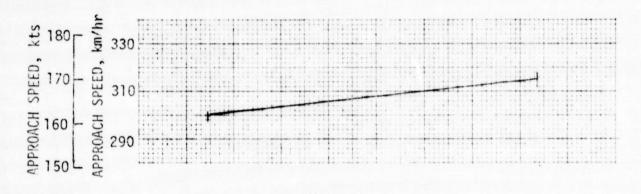
Figure 53. - Effect of Mach number on range and L/D.
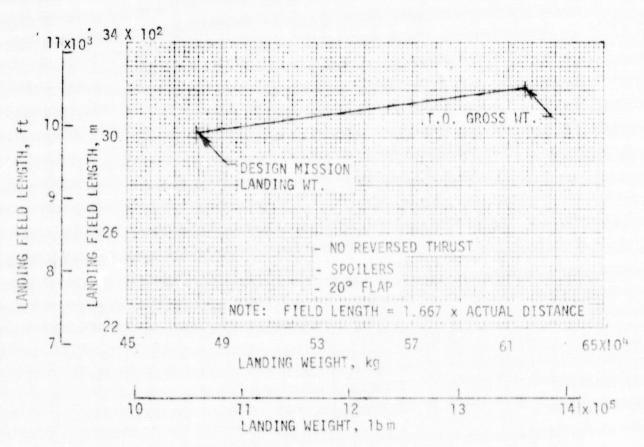
Figure 54. - Landing performance.
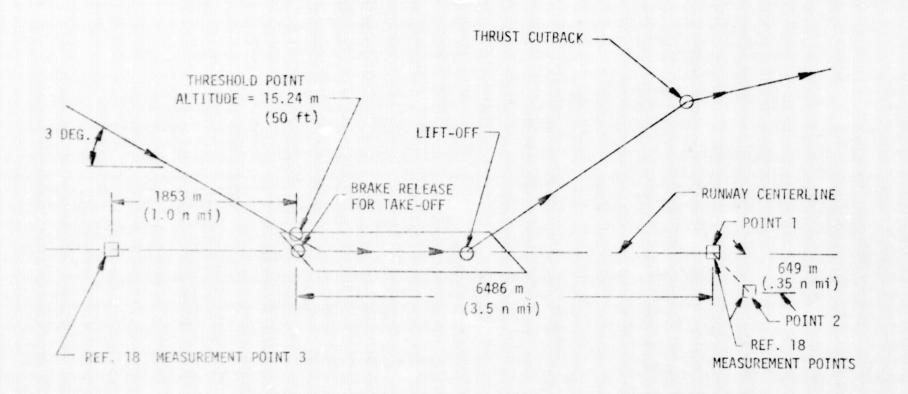
Figure 55.— Noise measurement locations for approach and take-off
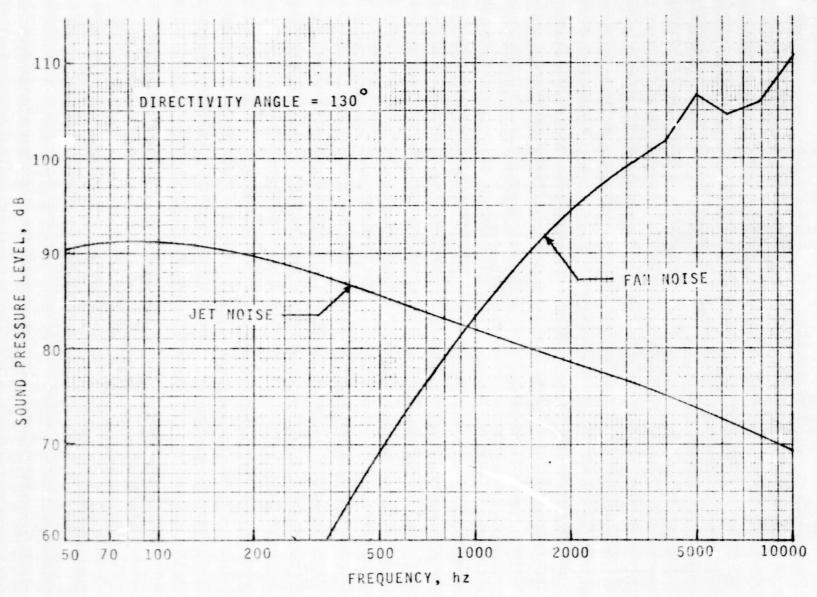
Figure 56. - Variation of engine take-off source levels with frequency.
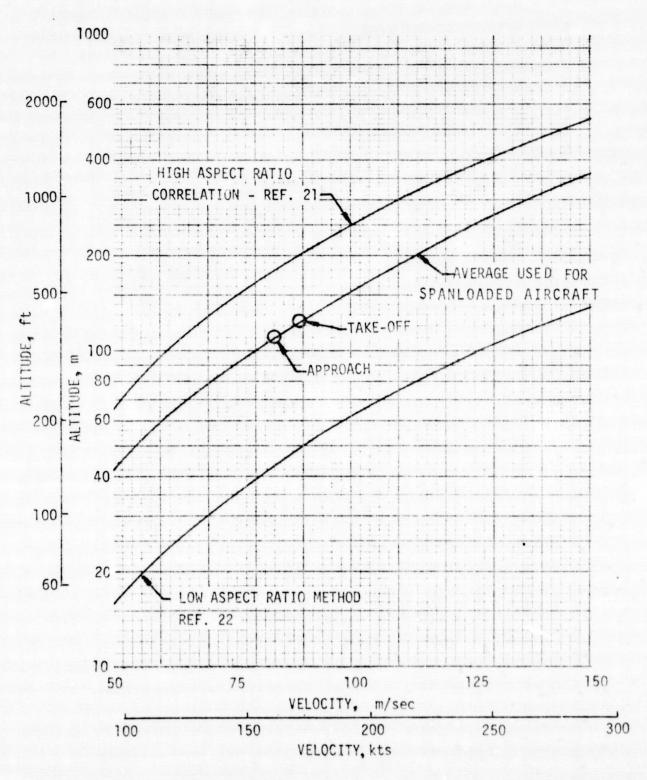
Figure 57. - Variation of altitude with velocity for spanloader airframe
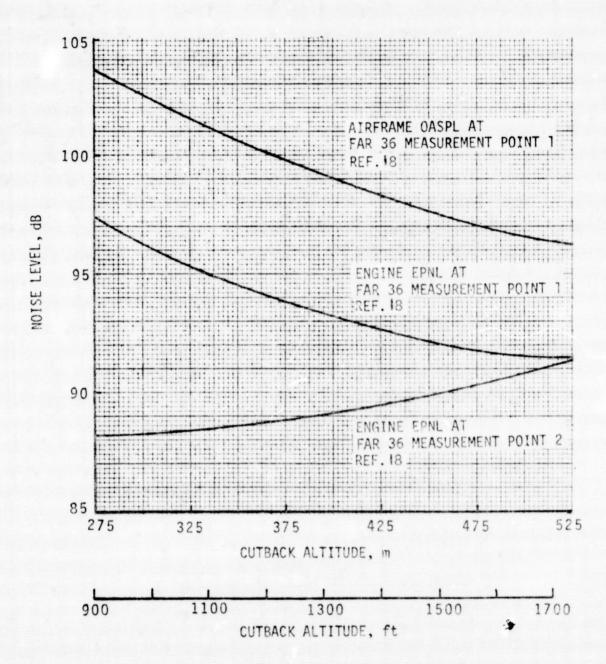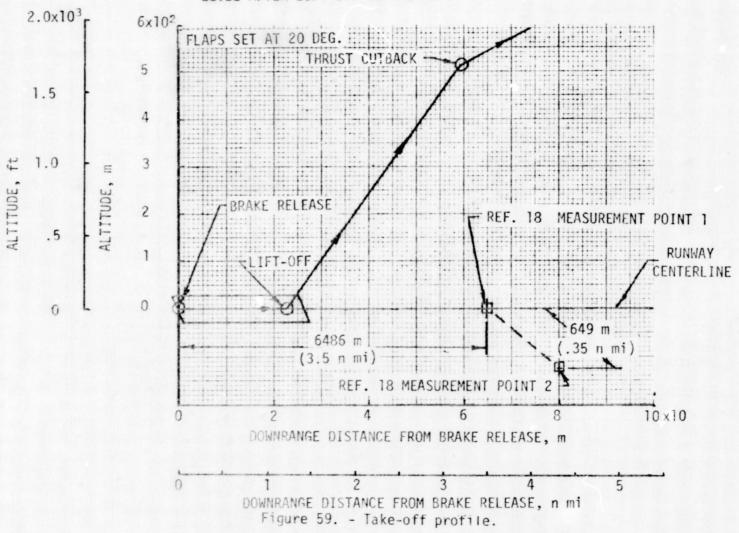noise level of 108 dB.

Figure 58. - Effect of cutback altitude on spanloader take-off noise levels.

SIDELINE NOISE IS MEASURED WHERE NOISE
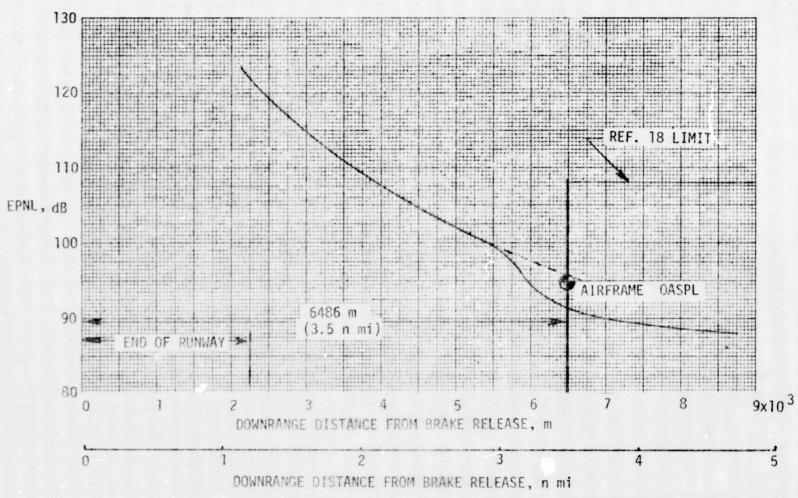LEVEL AFTER LIFT-OFF IS GREATEST

FLAPS SET AT 20 DEG.

THRUST CUTBACK

BRAKE RELEASE

REF. 18 MEASUREMENT POINT 1

RUNWAY CENTERLINE

LIFT-OFF

6486 m
(3.5 n mi)

649 m
(.35 n mi)

REF. 18 MEASUREMENT POINT 2

ALTITUDE, ft

ALTITUDE, m

DOWNRANGE DISTANCE FROM BRAKE RELEASE, m

DOWNRANGE DISTANCE FROM BRAKE RELEASE, n mi

Figure 59. - Take-off profile.

Figure 60. – Effective perceived noise level along runway centerline during take-off.
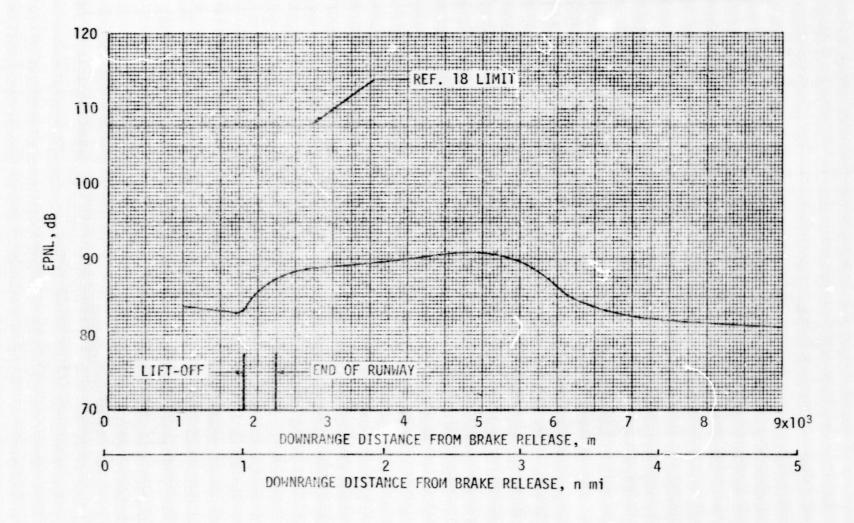
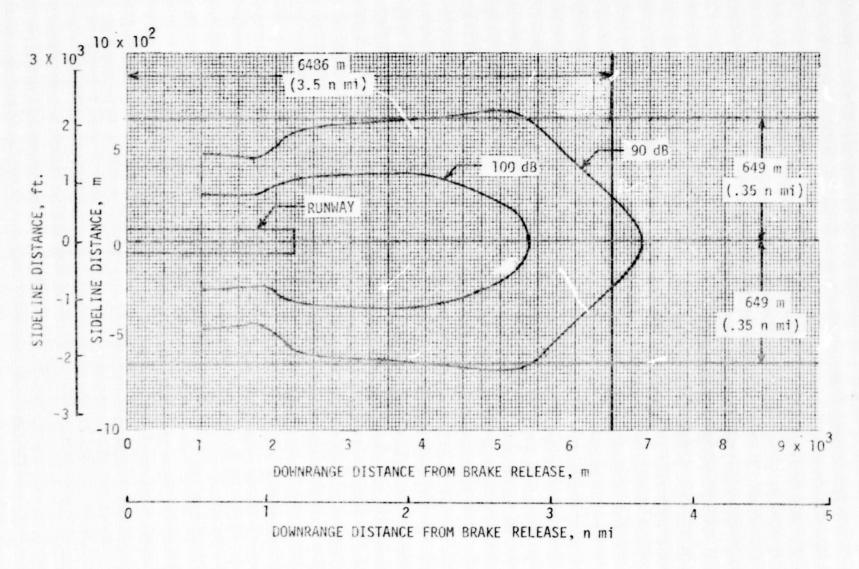Figure 61. - Effective perceived noise level along sideline during take-off.

Figure 62. - Constant engine effective perceived noise levels during take-off.